US 20070104974A1

(19) **United States**

(12) **Patent Application Publication** (10) **Pub. No.: US 2007/0104974 A1**

Natesan et al. (43) **Pub. Date: May 10, 2007**

(54) **NICKEL BASED ALLOYS TO PREVENT METAL DUSTING DEGRADATION**

(75) Inventors: **Krishnamurti Natesan**, Naperville, IL (US); **Zuotao Zeng**, Woodridge, IL (US)

Correspondence Address:
FOLEY & LARDNER LLP
321 NORTH CLARK STREET
SUITE 2800
CHICAGO, IL 60610-4764 (US)

(73) Assignee: **University of Chicago**

(21) Appl. No.: **11/443,566**

(22) Filed: **May 31, 2006**

Related U.S. Application Data

(60) Provisional application No. 60/686,480, filed on Jun. 1, 2005.

Publication Classification

(51) **Int. Cl.**
F01D 5/18 (2006.01)

(52) **U.S. Cl.** **428/586**; 428/674; 428/680

(57) **ABSTRACT**

An article of manufacture for reducing susceptibility of a metal pipe to metal dusting degradation. The article includes a multi-layer tubing having an alloy layer and a copper layer. The alloy layer can include a Ni based, an Al based and an Fe based alloy layer. In addition, layers of chrome oxide, spinel and aluminum oxide can be used.

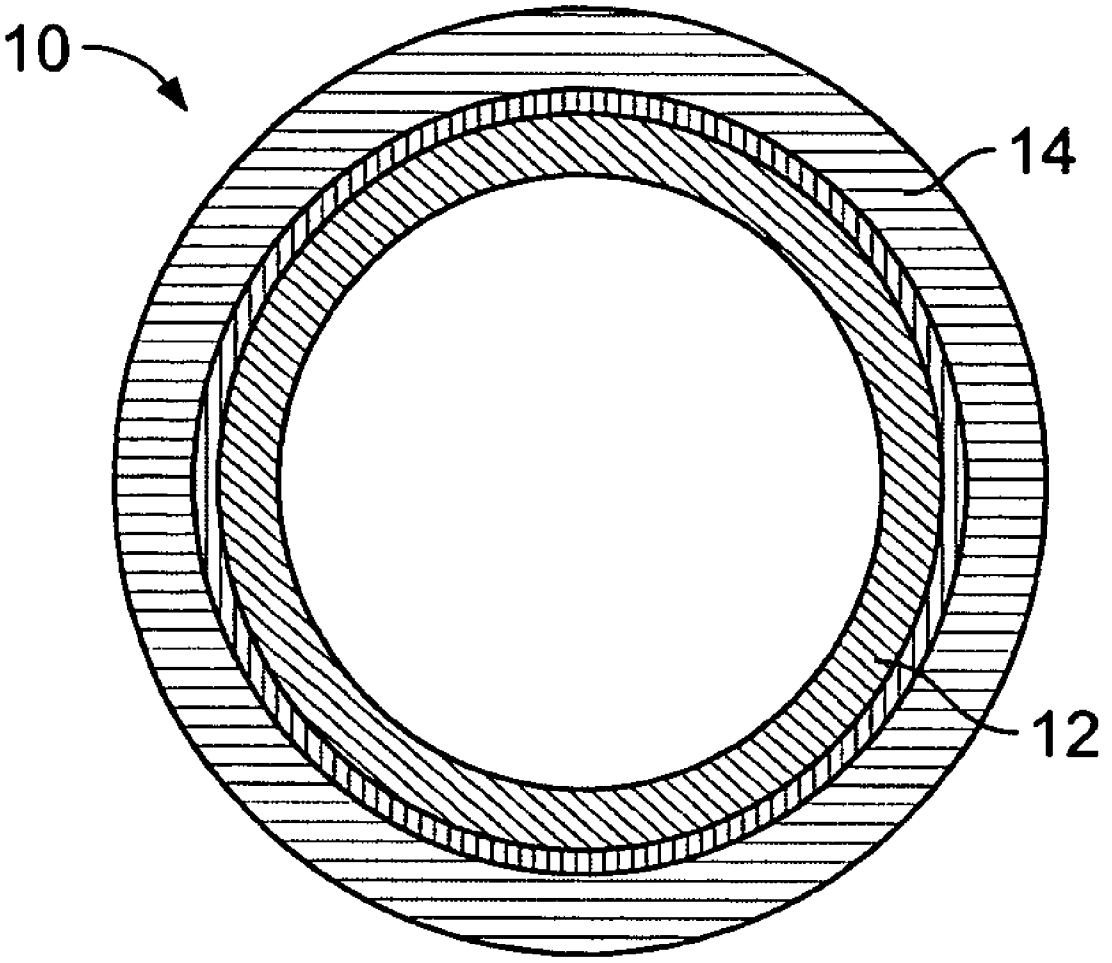

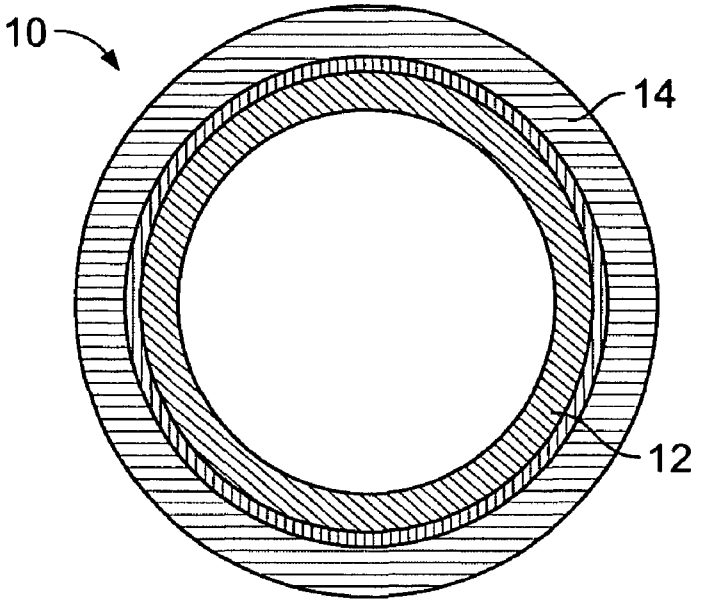

FIG. 1

Alloy 800

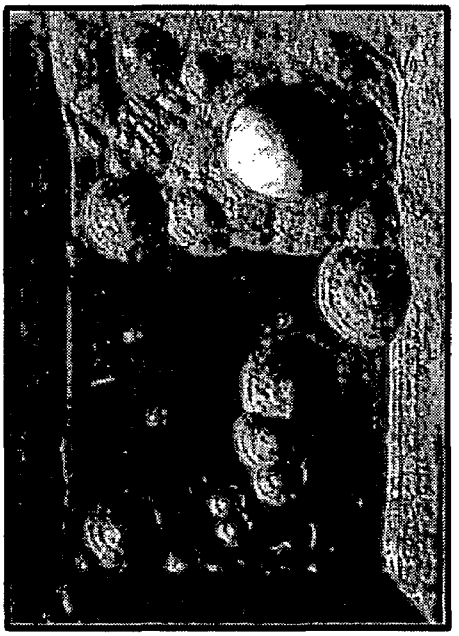

FIG. 2A

Alloy 321

FIG. 2B

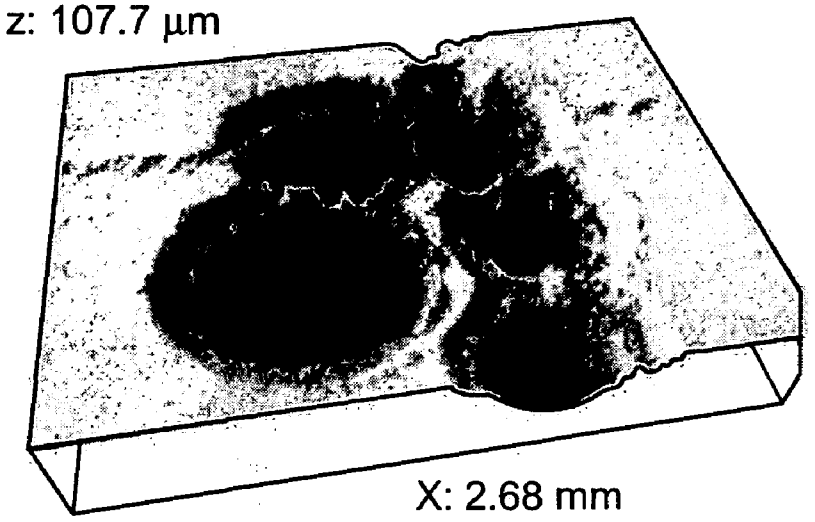

FIG. 3

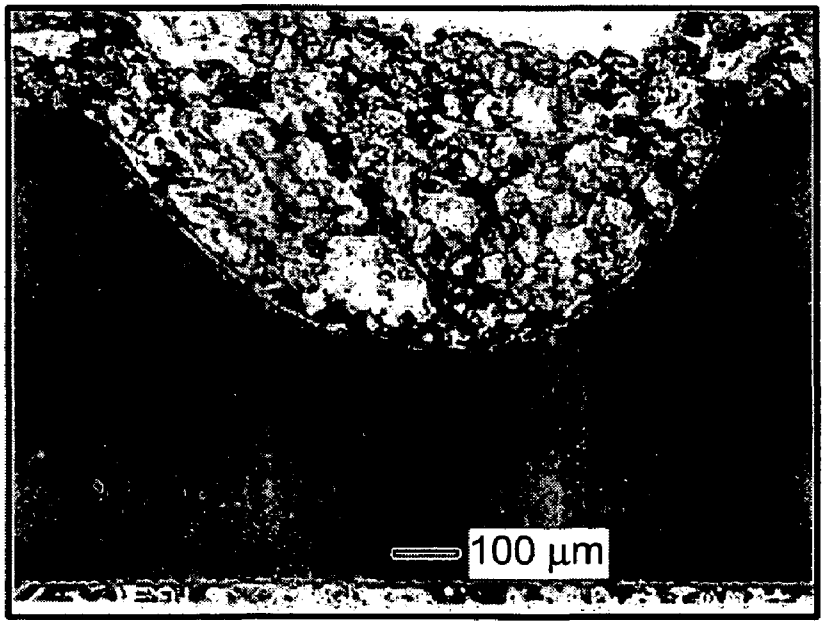

FIG. 4

FIG. 5A

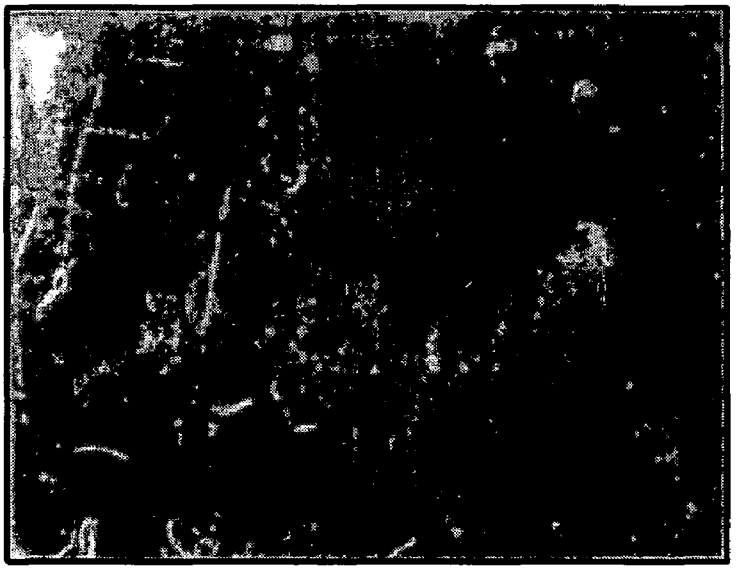

FIG. 5B

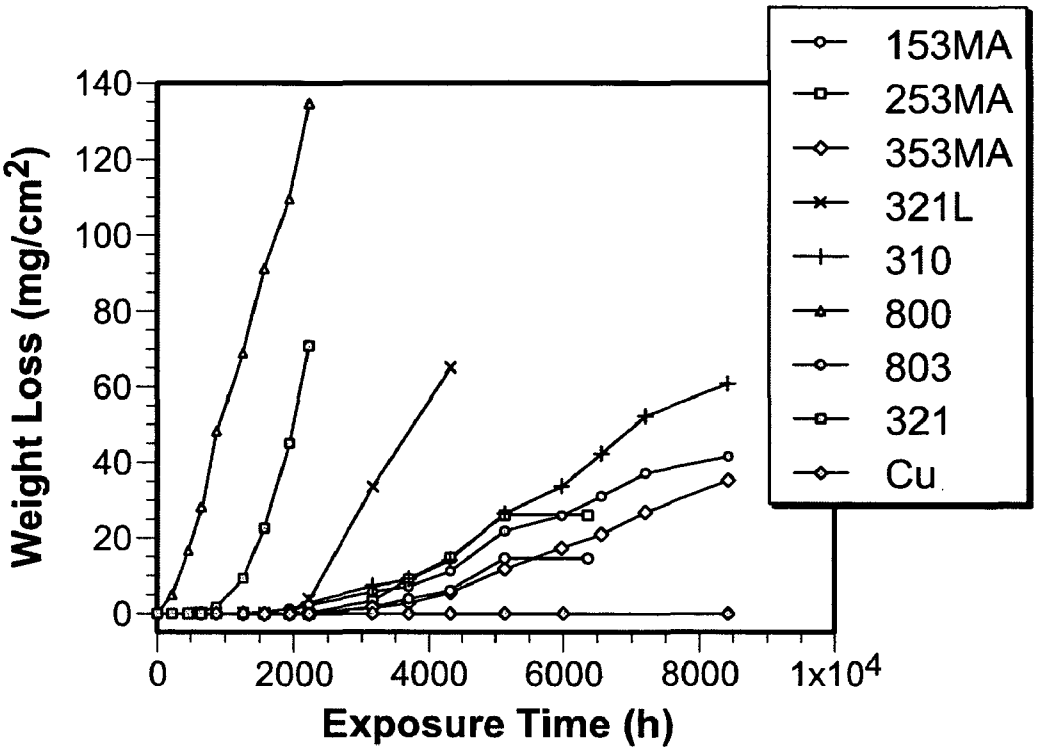
153MA
253MA
353MA
321L
310
800
803
321
Cu
Weight Loss (mg/cm2)
Exposure Time (h)
0
20
40
60
80
100
120
140
0
2000
4000
6000
8000
1x10^4

FIG. 6

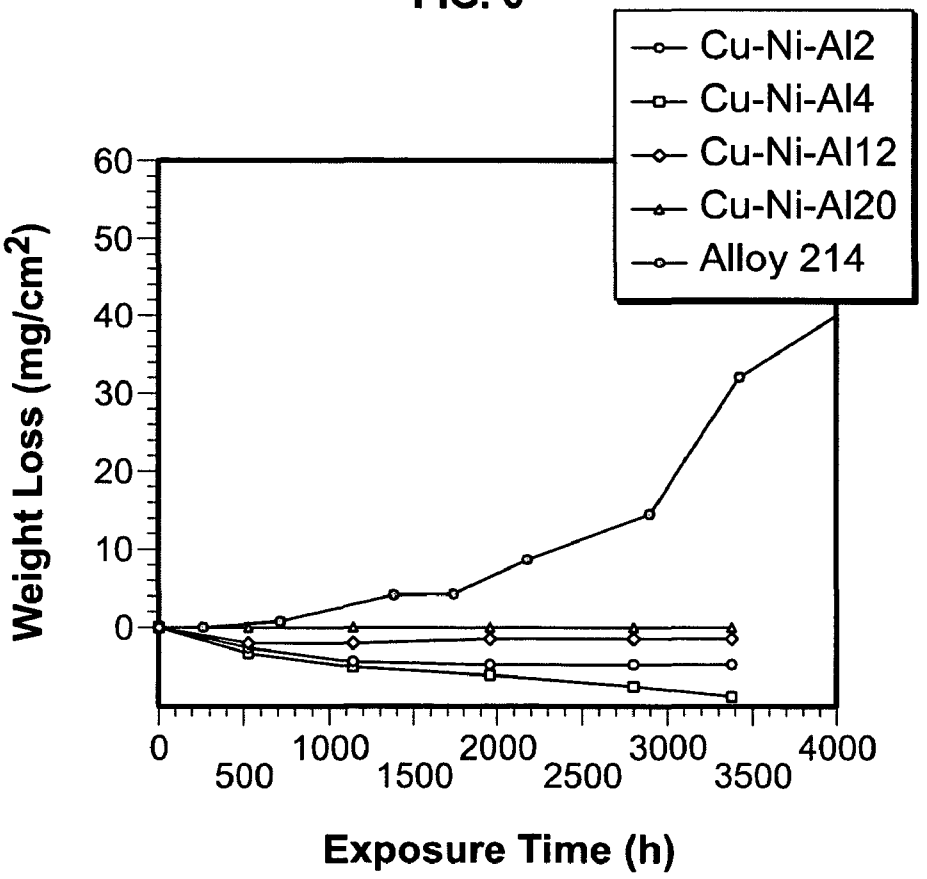
Cu-Ni-Al2
Cu-Ni-Al4
Cu-Ni-Al12
Cu-Ni-Al20
Alloy 214
Weight Loss (mg/cm2)
Exposure Time (h)
0
10
20
30
40
50
60
0
500
1000
1500
2000
2500
3000
3500
4000

FIG. 7

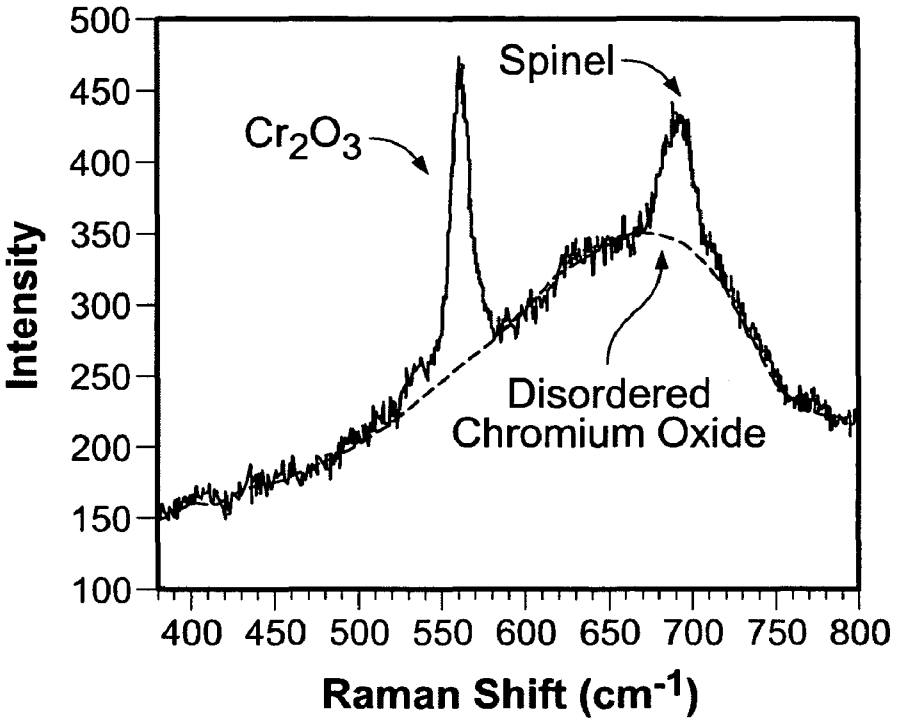
Intensity
500
450
400
350
300
250
200
150
100
400 450 500 550 600 650 700 750 800
Raman Shift (cm-1)
Spinel
Cr2O3
Disordered
Chromium Oxide

FIG. 8

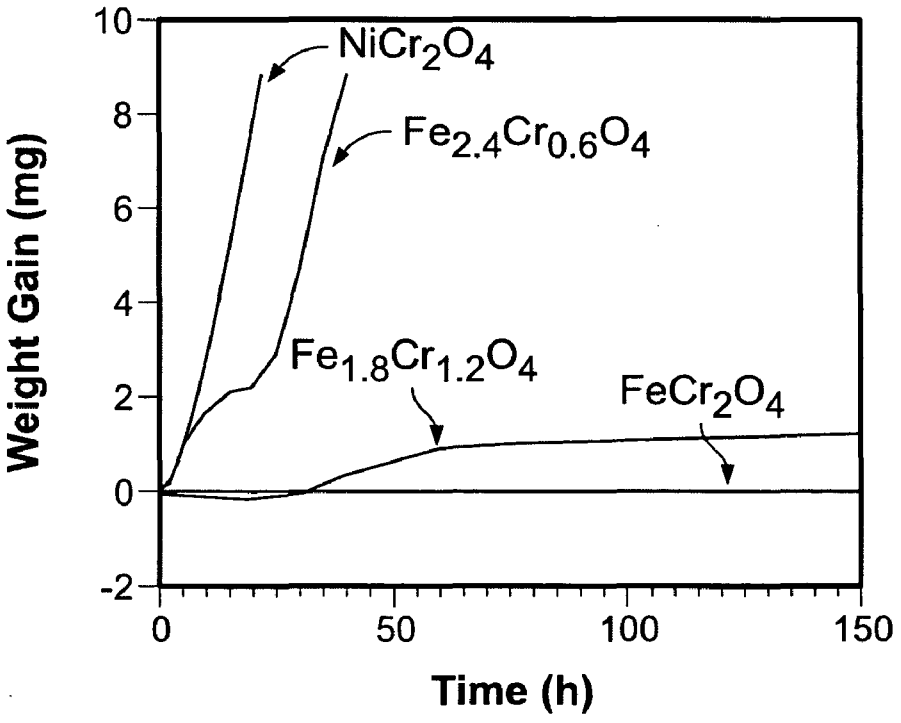
Weight Gain (mg)
10
8
6
4
2
0
-2
0 50 100 150
Time (h)
NiCr2O4
Fe2.4Cr0.6O4
Fe1.8Cr1.2O4
FeCr2O4

FIG. 9

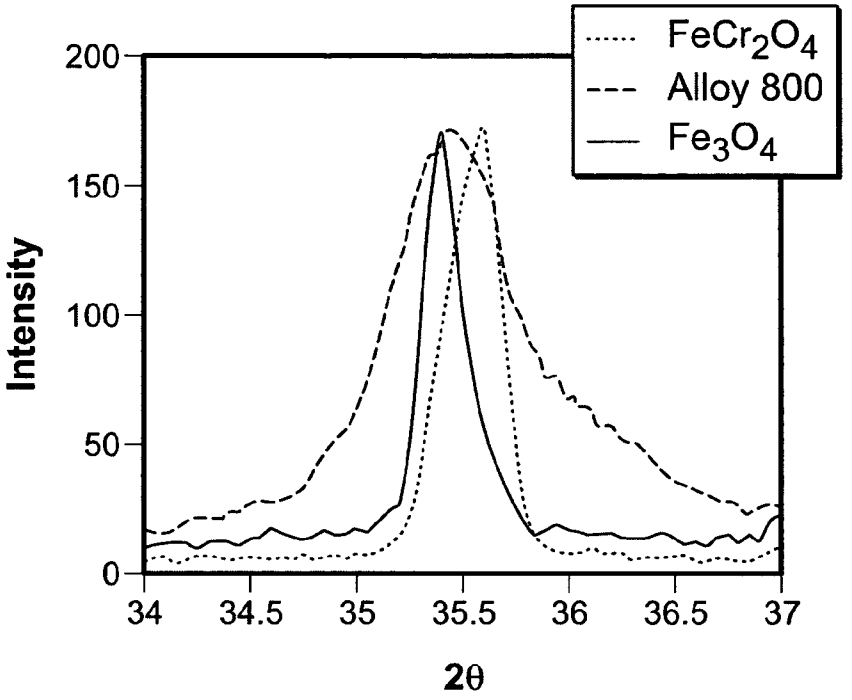

FIG. 10

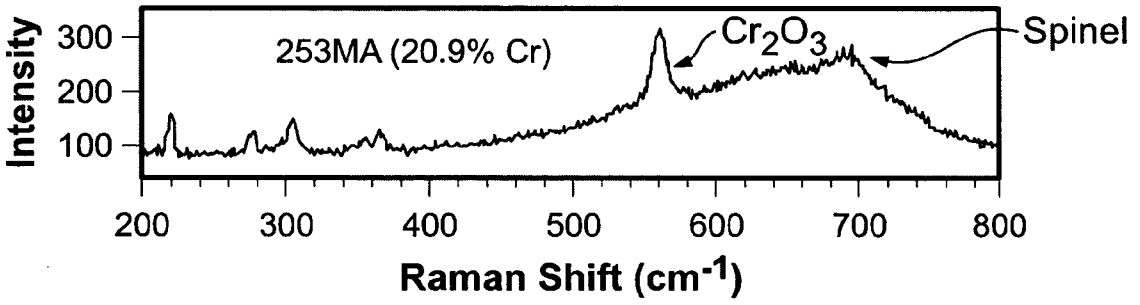

FIG. 11A

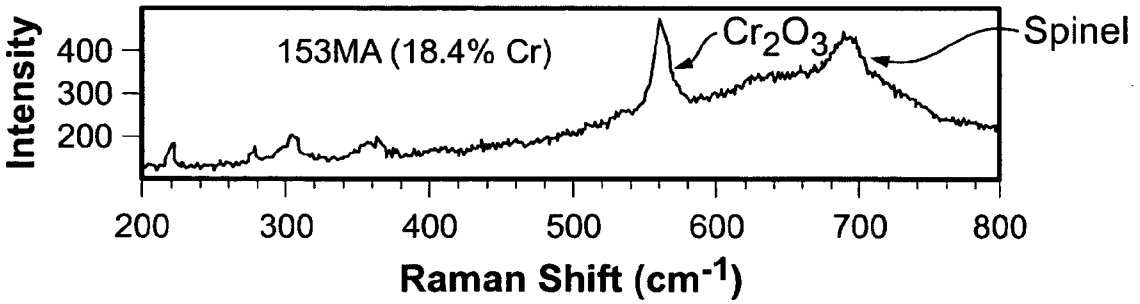

FIG. 11B

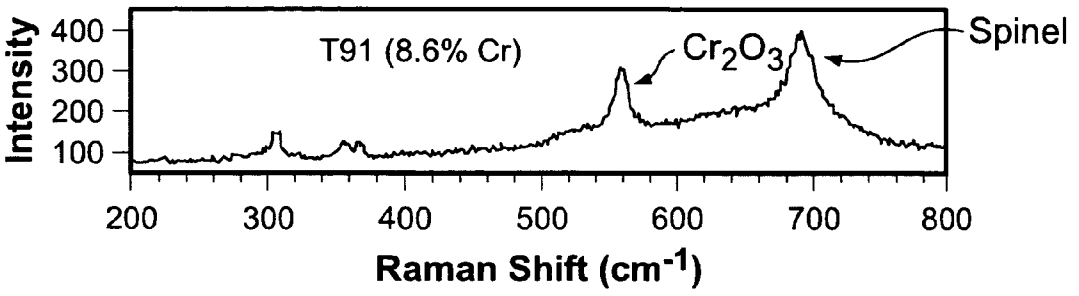

FIG. 11C

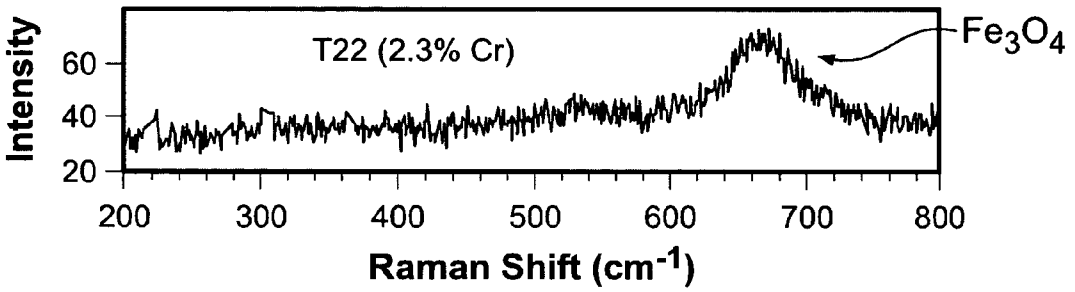

FIG. 11D

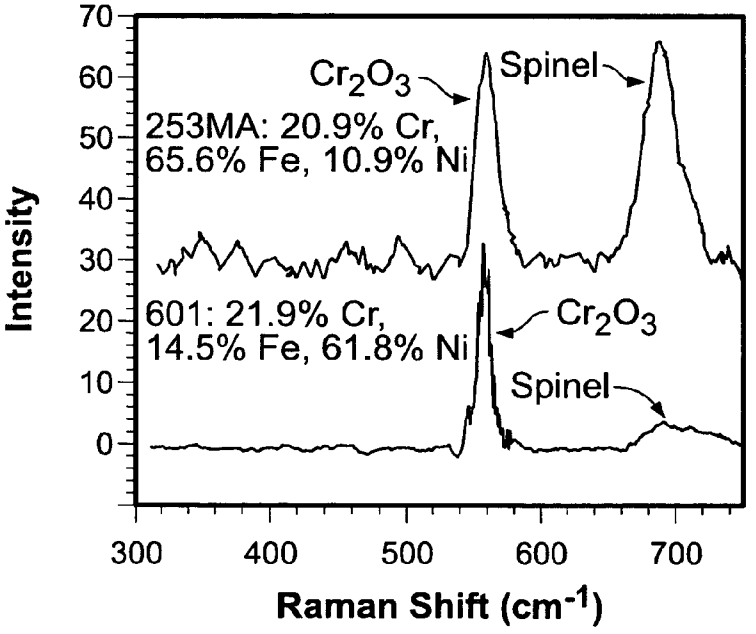

FIG. 12

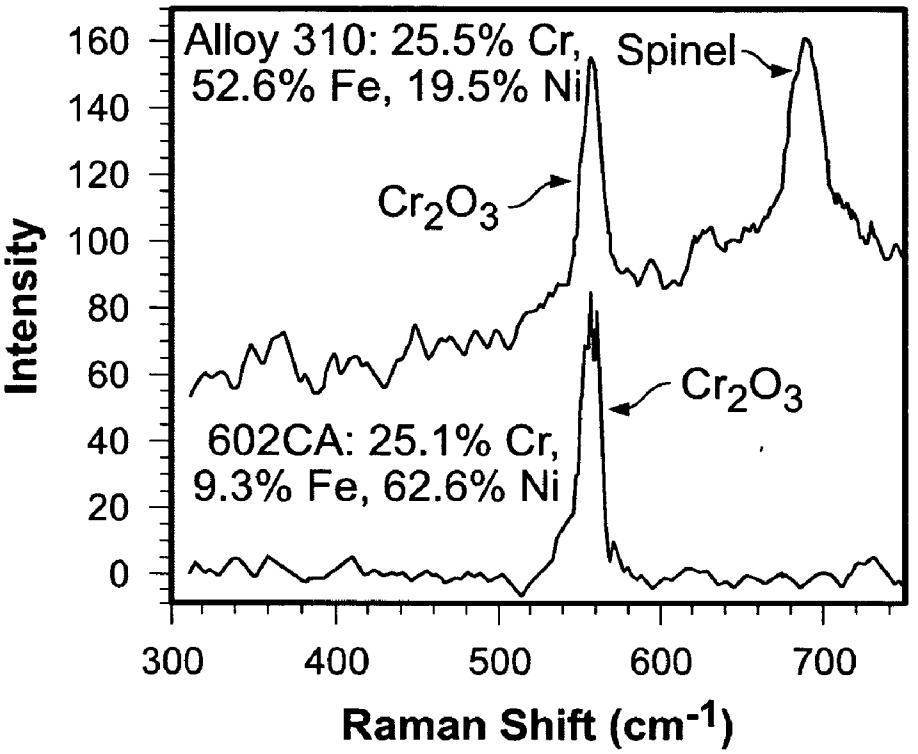
Alloy 310: 25.5% Cr,
52.6% Fe, 19.5% Ni
Spinel
Cr_2O_3
Cr_2O_3
602CA: 25.1% Cr,
9.3% Fe, 62.6% Ni
Intensity
Raman Shift (cm^{-1})
0
20
40
60
80
100
120
140
160
300
400
500
600
700

FIG. 13

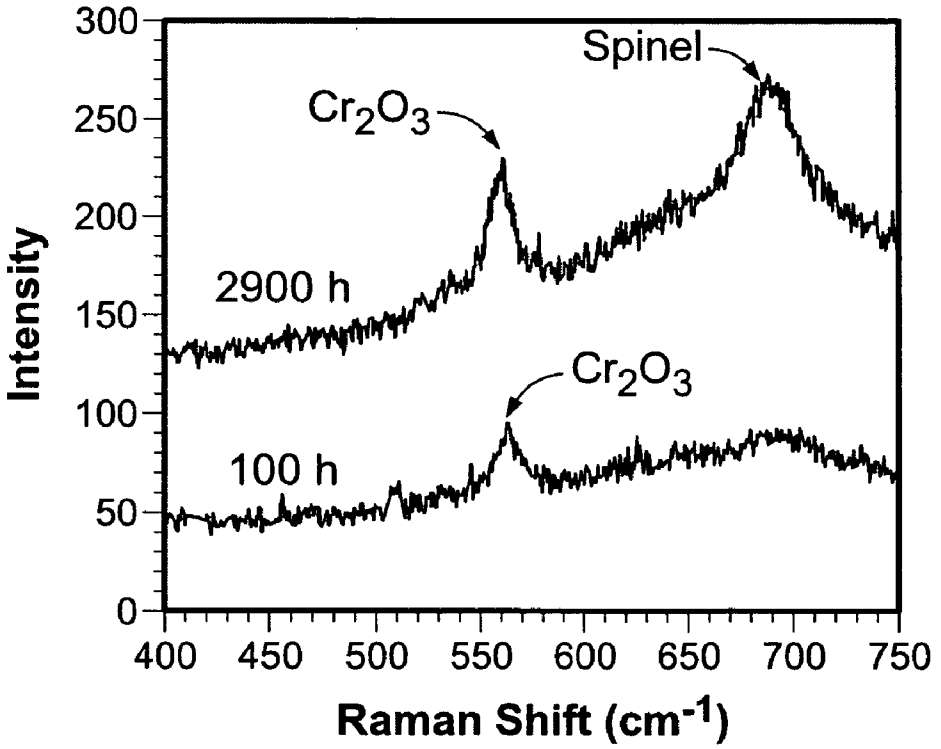
Spinel
Cr_2O_3
2900 h
Cr_2O_3
100 h
Intensity
Raman Shift (cm^{-1})
0
50
100
150
200
250
300
400
450
500
550
600
650
700
750

FIG. 14

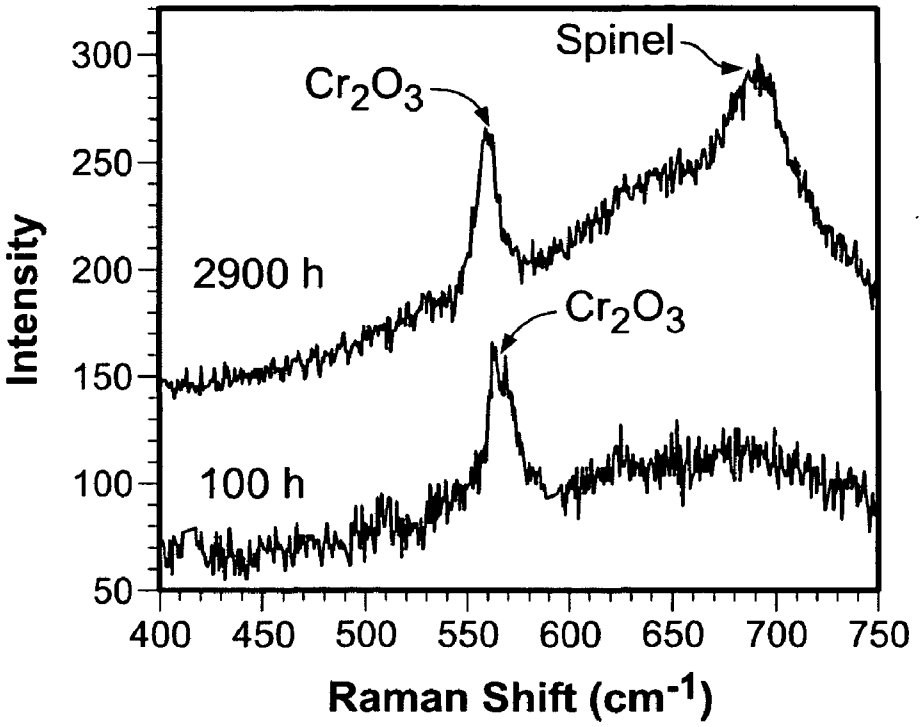
Spinel
Cr_2O_3
2900 h
Cr_2O_3
100 h
Intensity
300
250
200
150
100
50
400
450
500
550
600
650
700
750
Raman Shift (cm^{-1})

FIG. 15

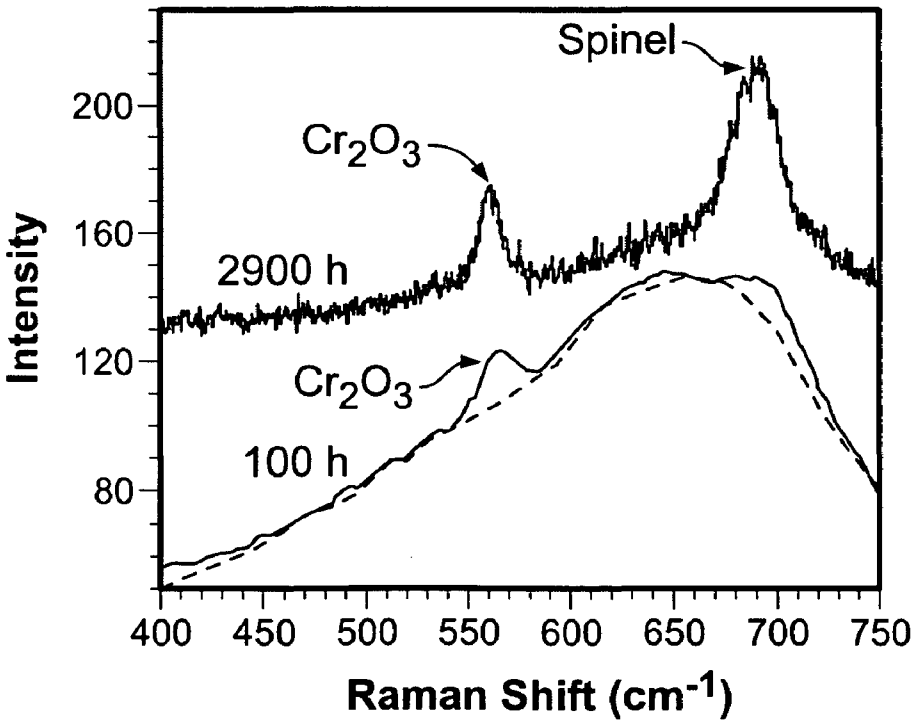
Spinel
Cr_2O_3
2900 h
Cr_2O_3
100 h
Intensity
200
160
120
80
400
450
500
550
600
650
700
750
Raman Shift (cm^{-1})

FIG. 16

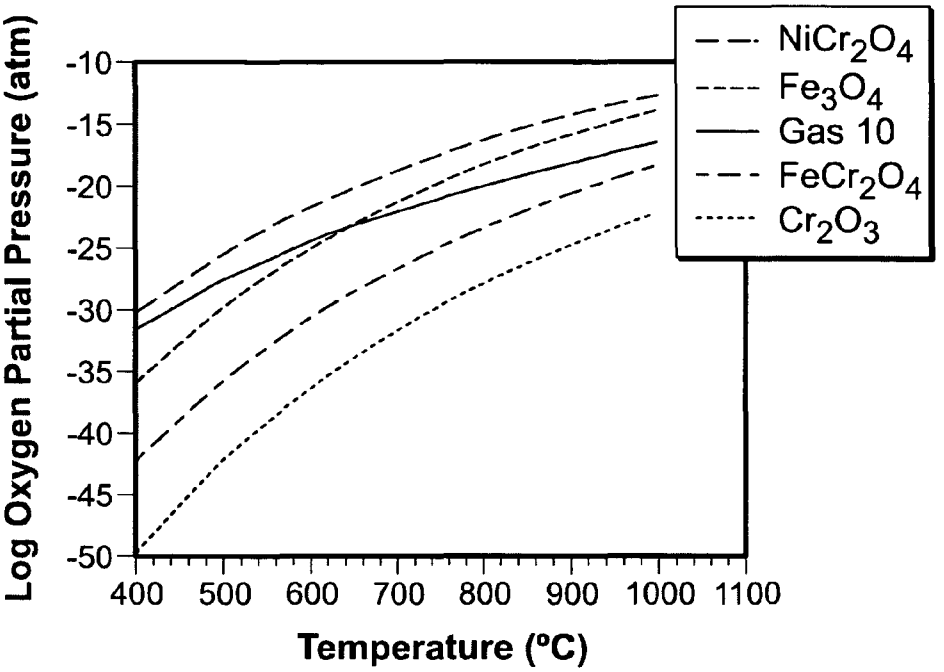

FIG. 17

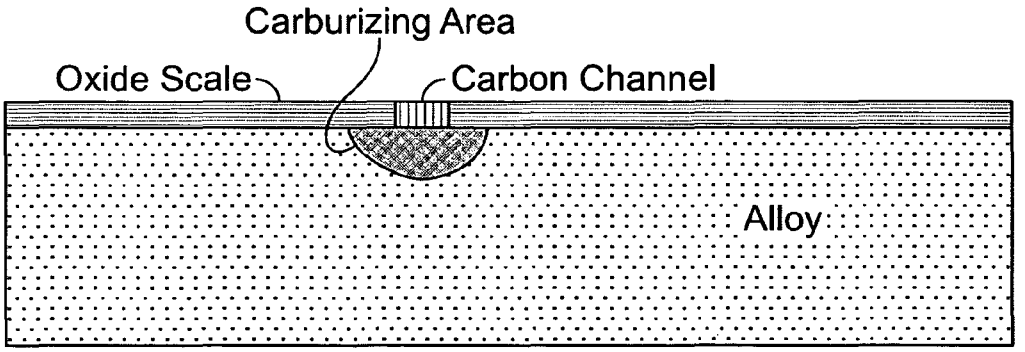

FIG. 18A

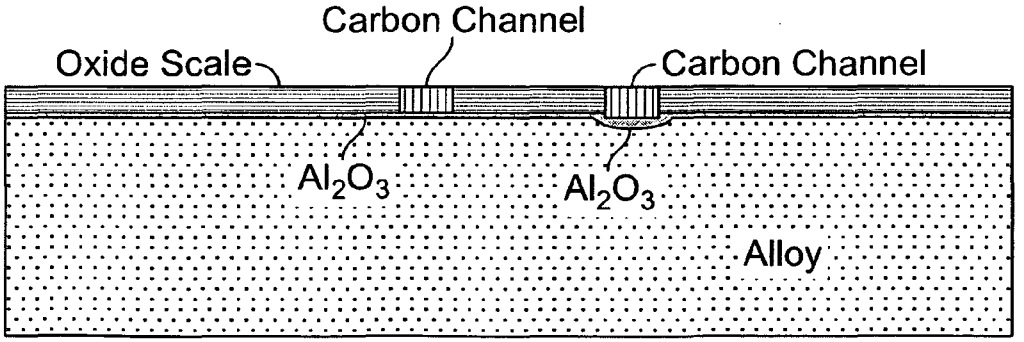

FIG. 18B

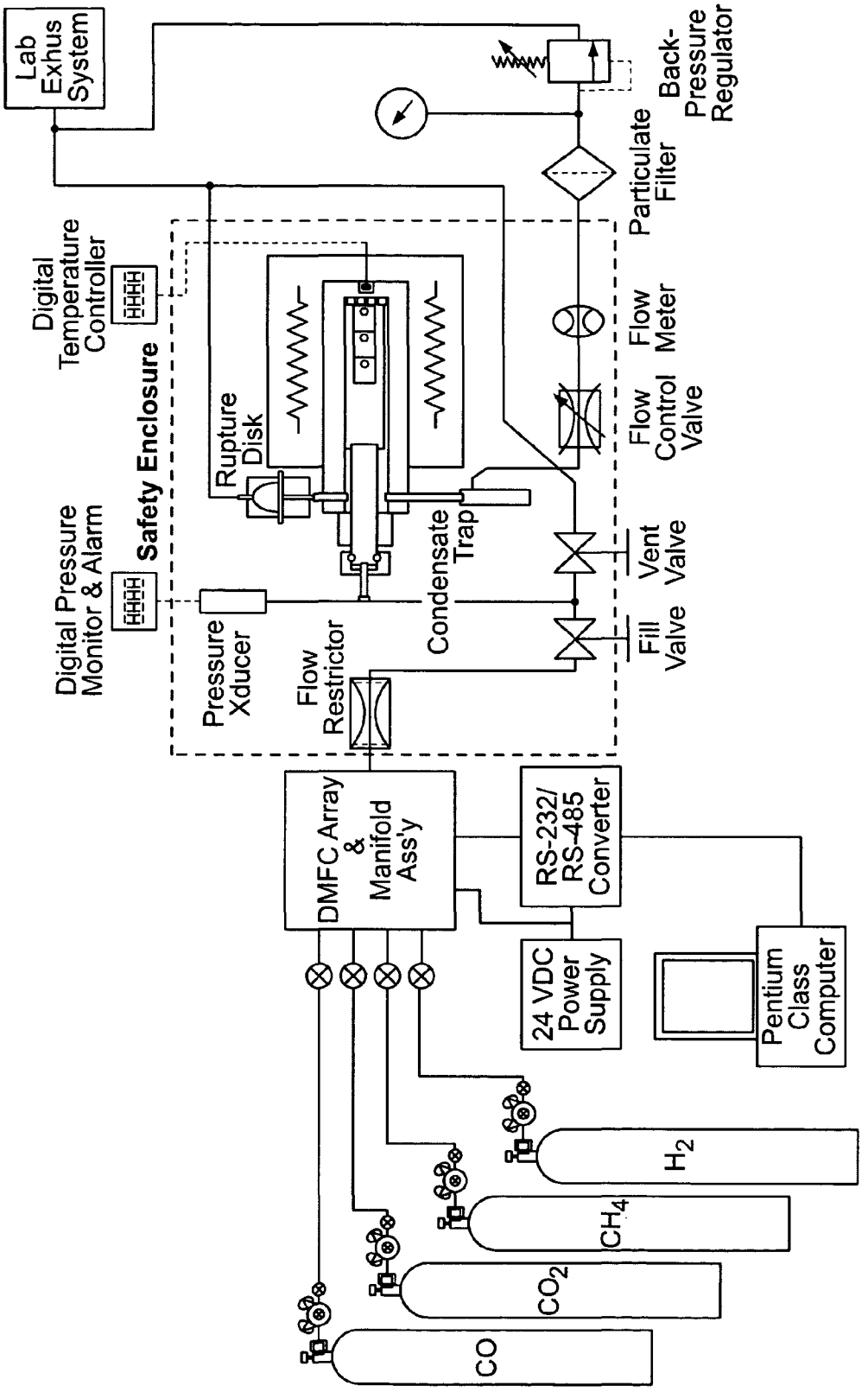
Lab Exhus System
Back-Pressure Regulator
Particulate Filter
Digital Temperature Controller
Flow Meter
Flow Control Valve
Rupture Disk
Safety Enclosure
Digital Pressure Monitor & Alarm
Condensate Trap
Vent Valve
Fill Valve
Pressure Xducer
Flow Restrictor
DMFC Array & Manifold Ass'y
RS-232/ RS-485 Converter
24 VDC Power Supply
Pentium Class Computer
H_2
CH_4
CO_2
CO

FIG. 19

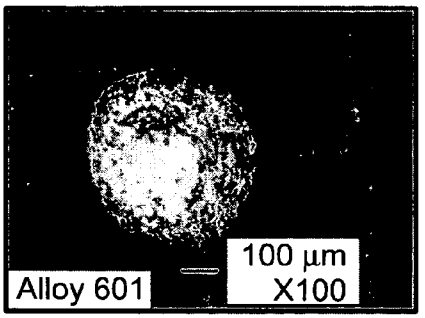

FIG. 20A

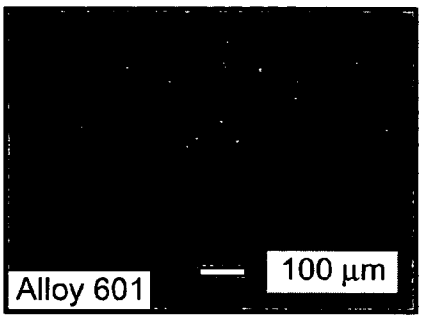

FIG. 20B

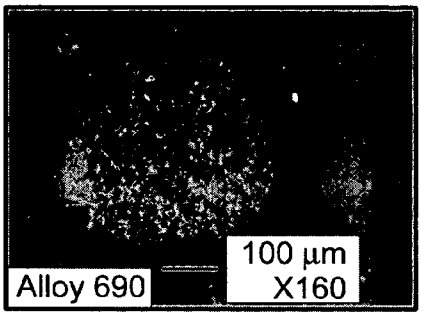

FIG. 20C

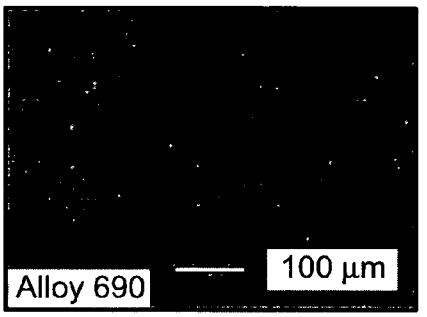

FIG. 20D

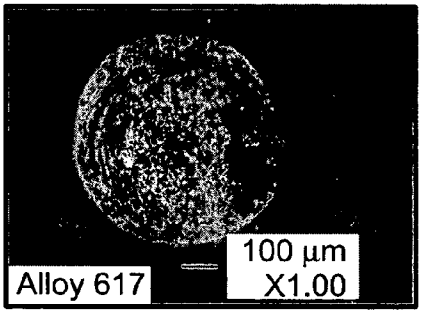

FIG. 20E

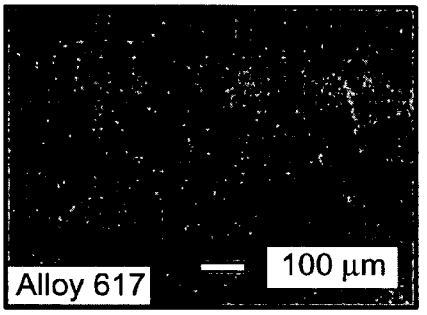

FIG. 20F

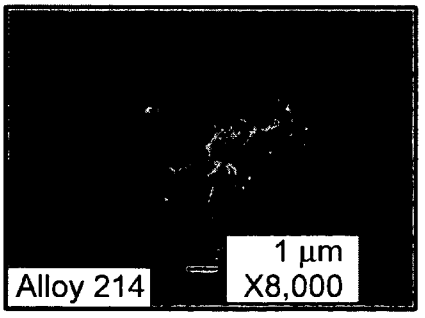

FIG. 20G

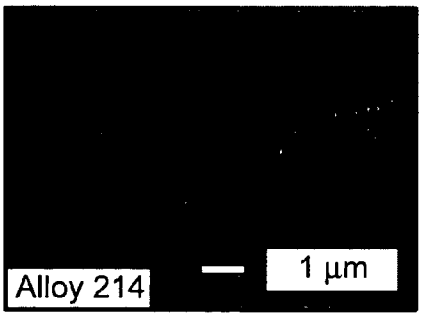

FIG. 20H

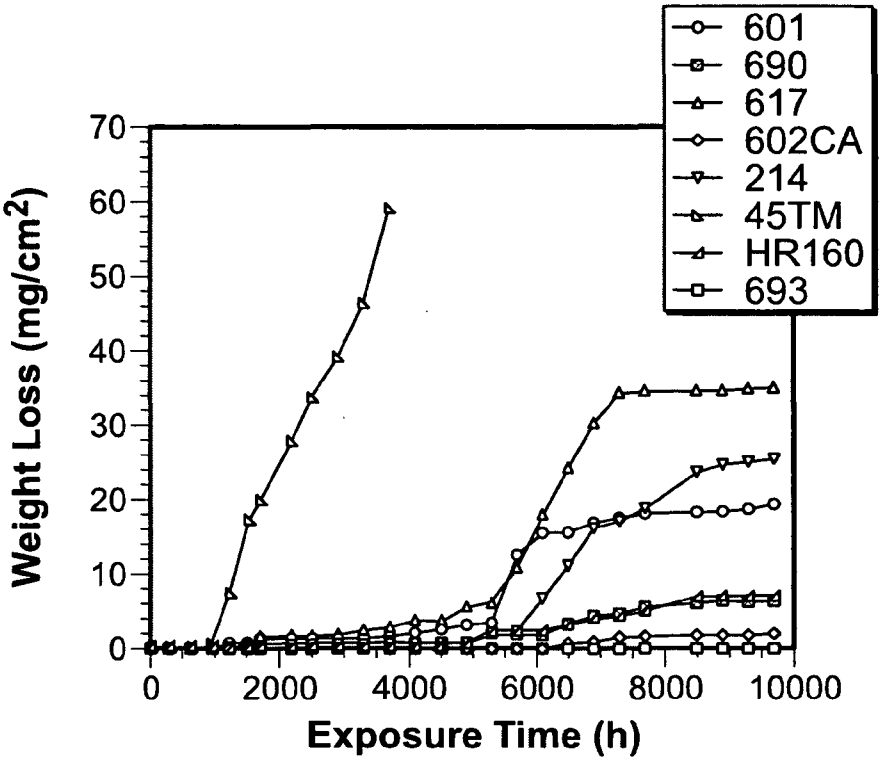

FIG. 21

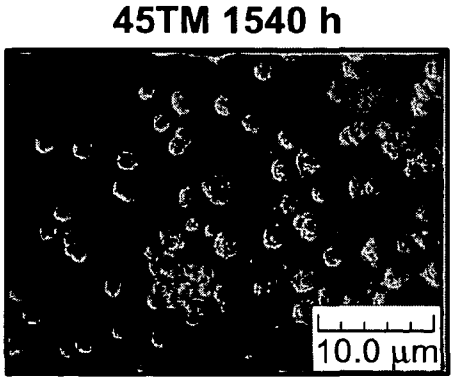

FIG. 22A

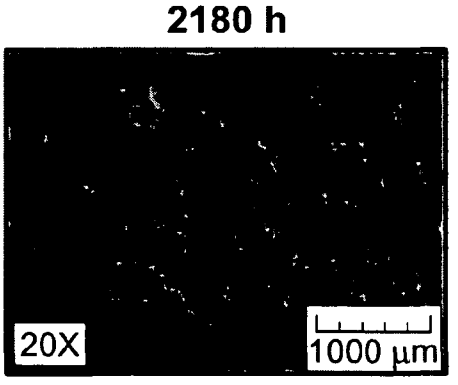

FIG. 22B

2500 h

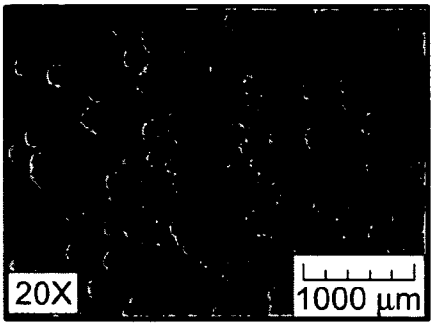

FIG. 22C

3300 h

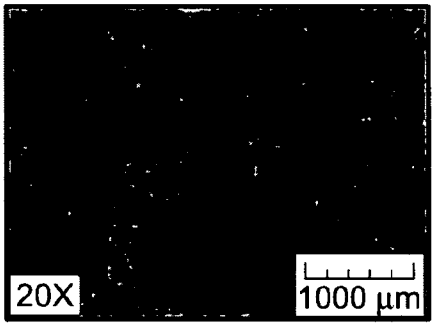

FIG. 22D

Alloy 690 2900 h

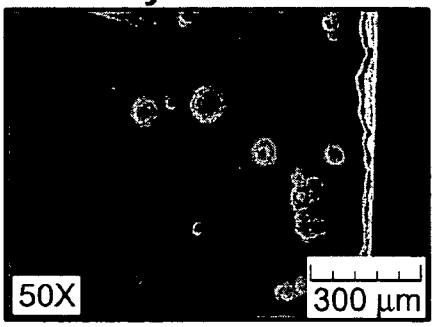

FIG. 22E

4100 h

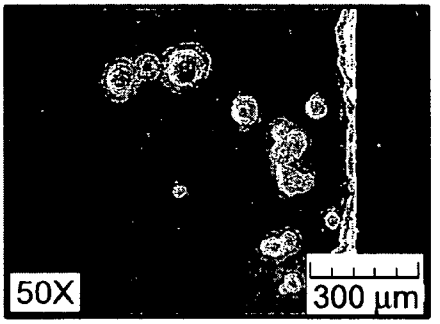

FIG. 22F

7300 h

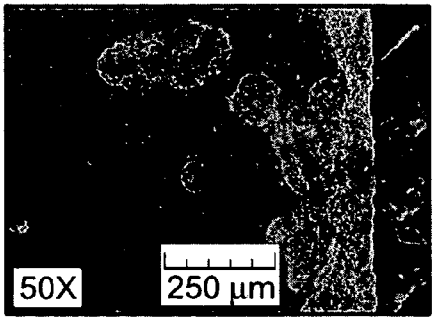

FIG. 22G

9300 h

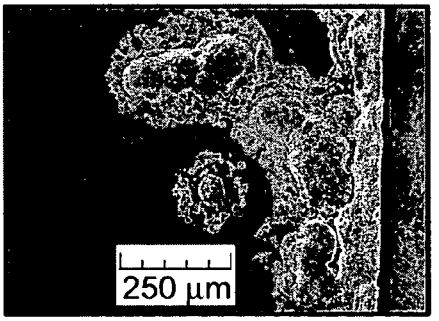

FIG. 22H

Alloy 617 2900 h

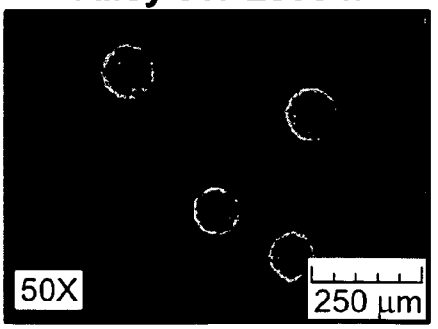

FIG. 22I

4100 h

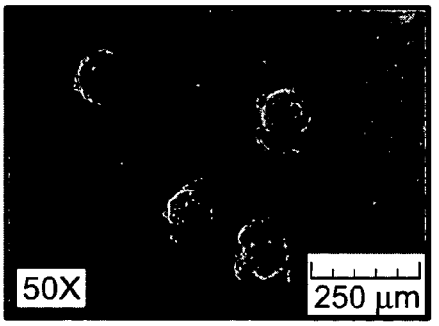

FIG. 22J

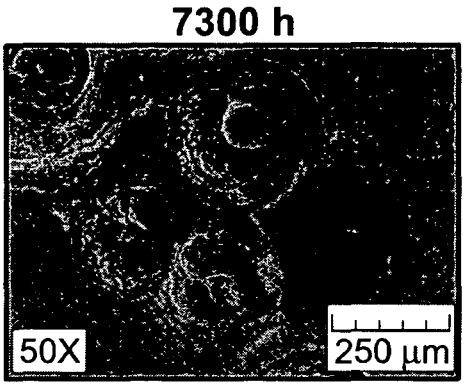

FIG. 22K

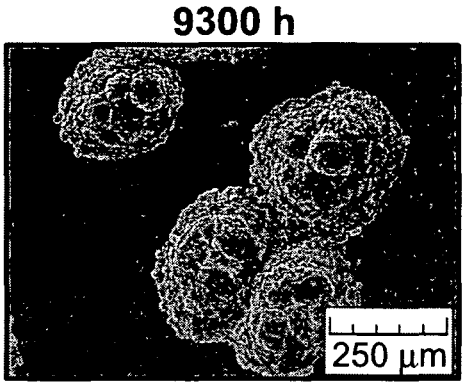

FIG. 22L

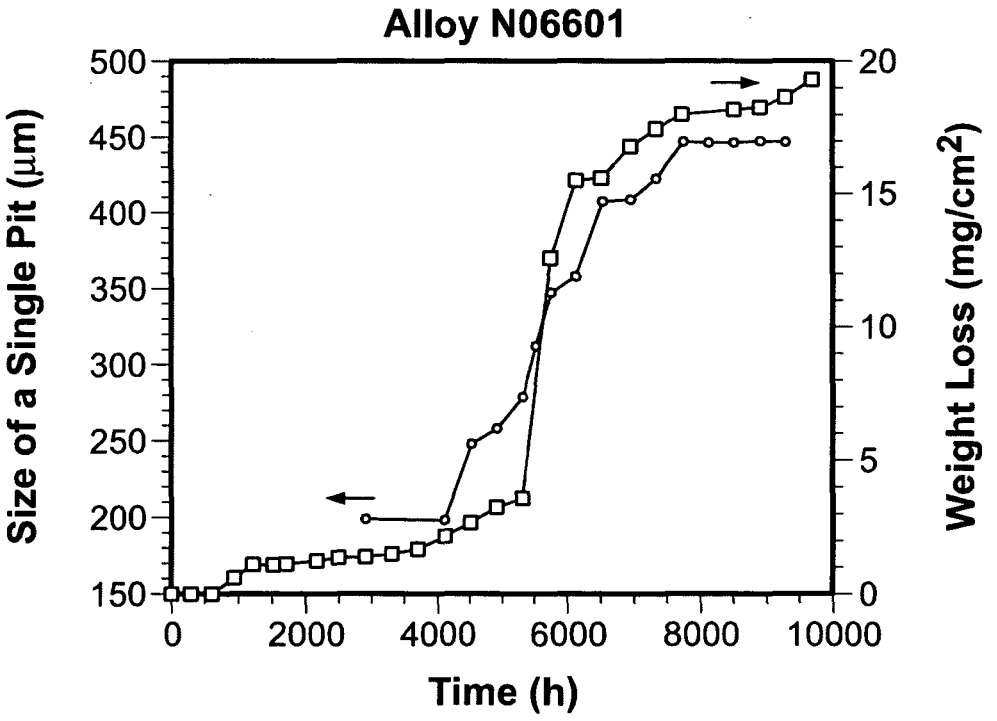

FIG. 23A

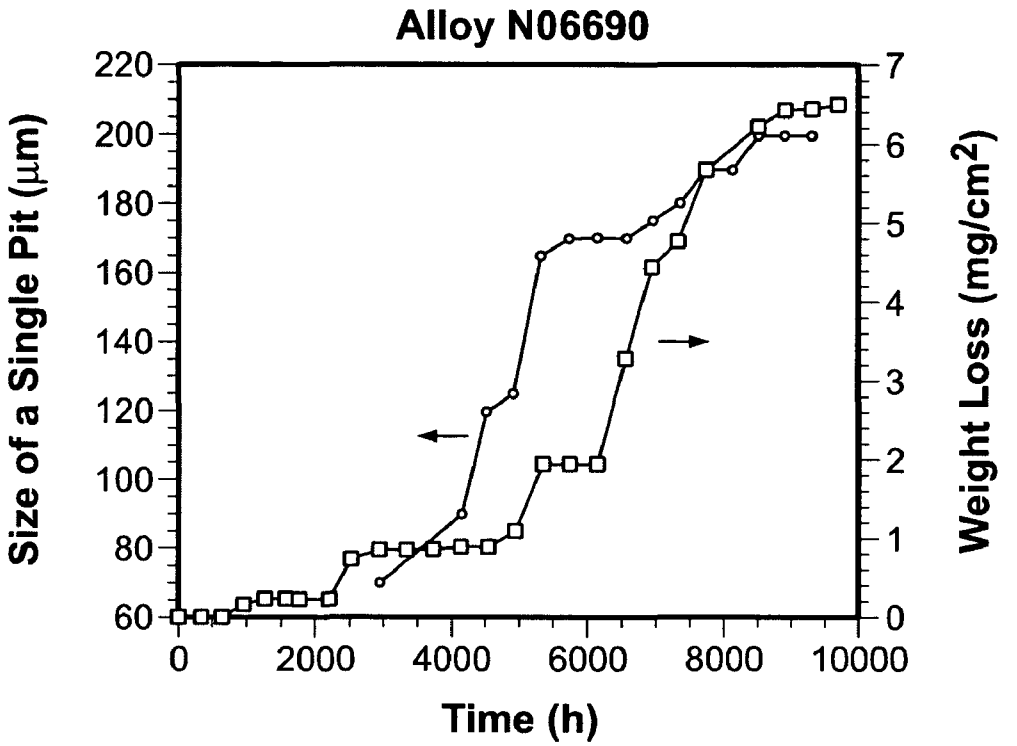

FIG. 23B

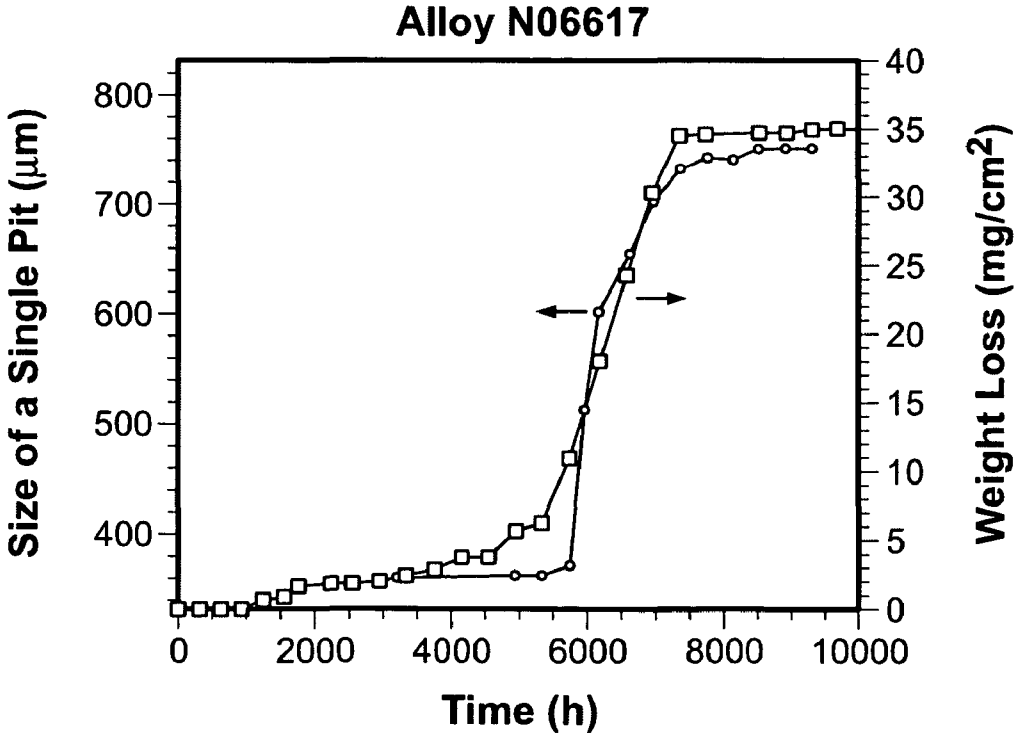

FIG. 23C

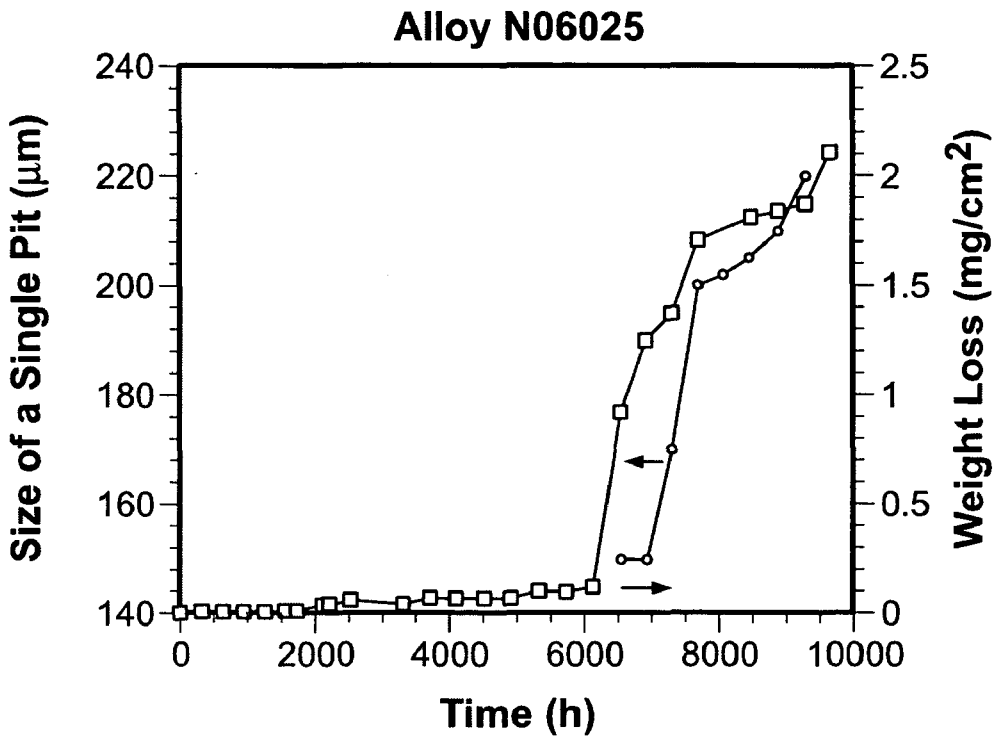

FIG. 23D

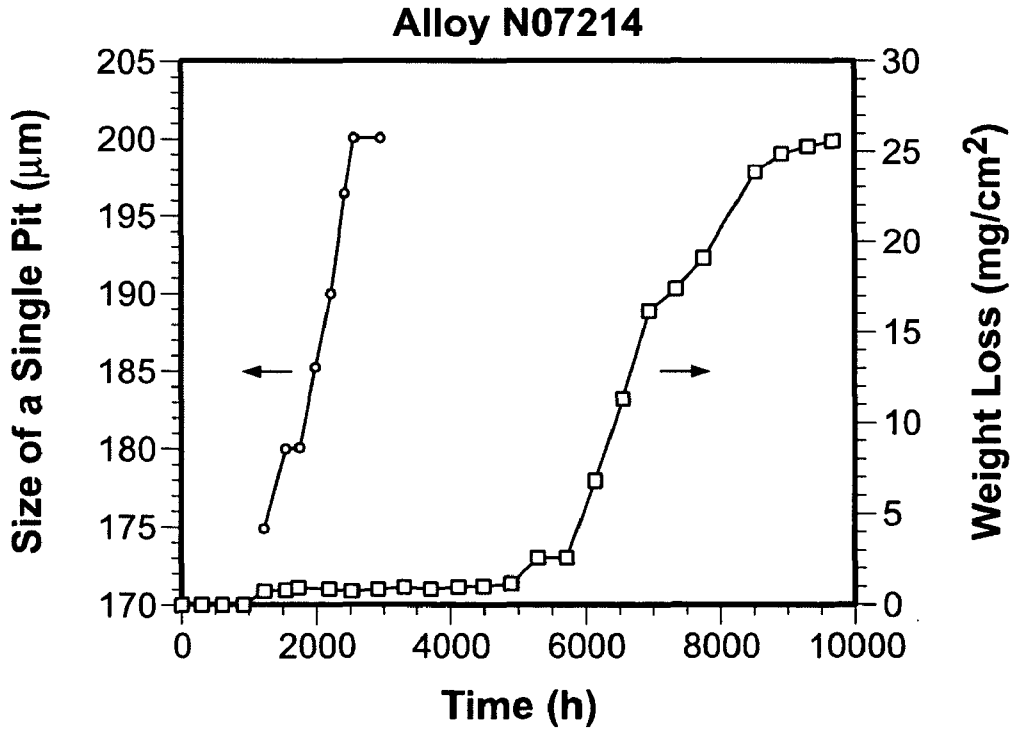

FIG. 23E

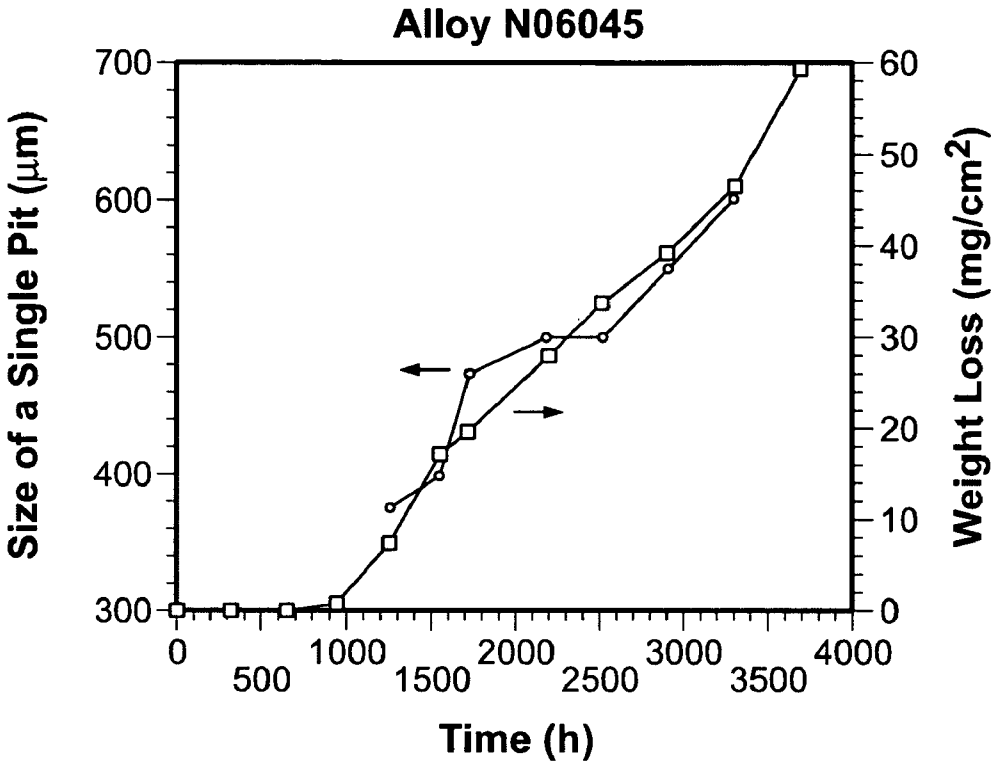

FIG. 23F

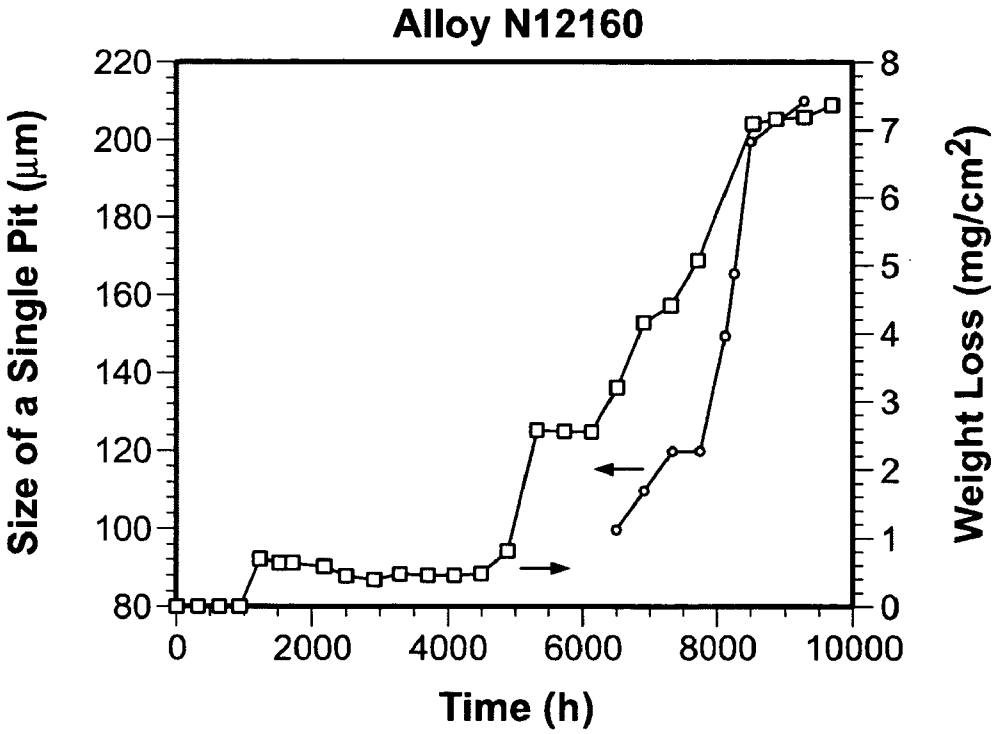

FIG. 23G

601

FIG. 24A

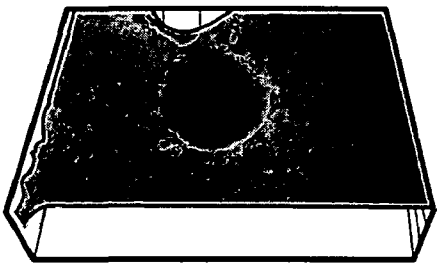

690

FIG. 24B

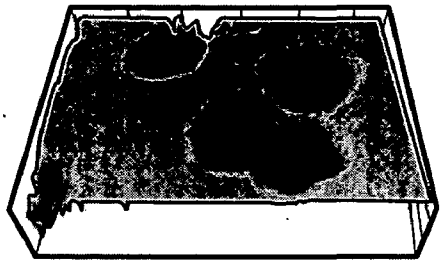

617

FIG. 24C

602CA

FIG. 24D

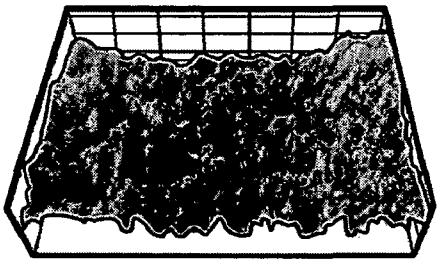

214

FIG. 24E

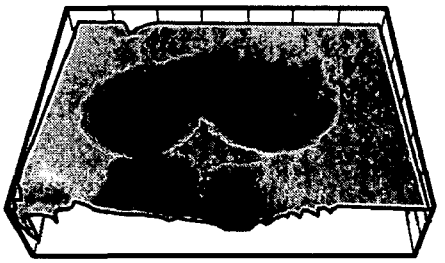

45TM

FIG. 24F

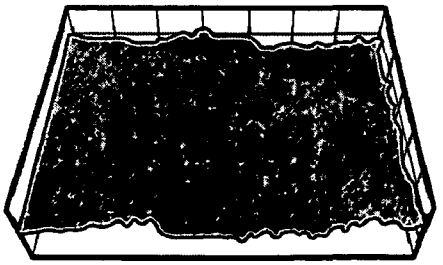

HR160

FIG. 24G

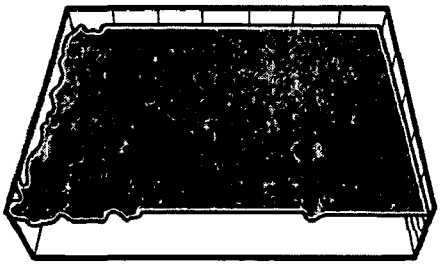

693

FIG. 24H

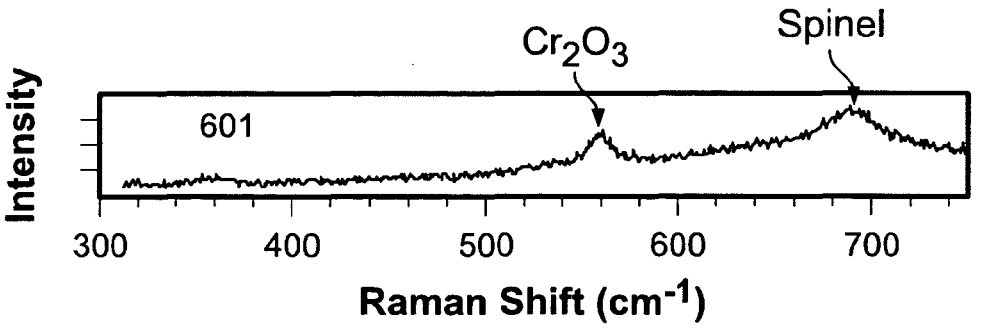

FIG. 25A

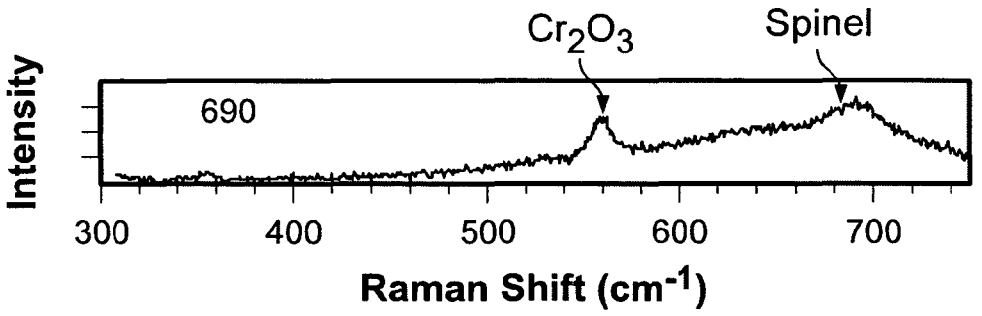

FIG. 25B

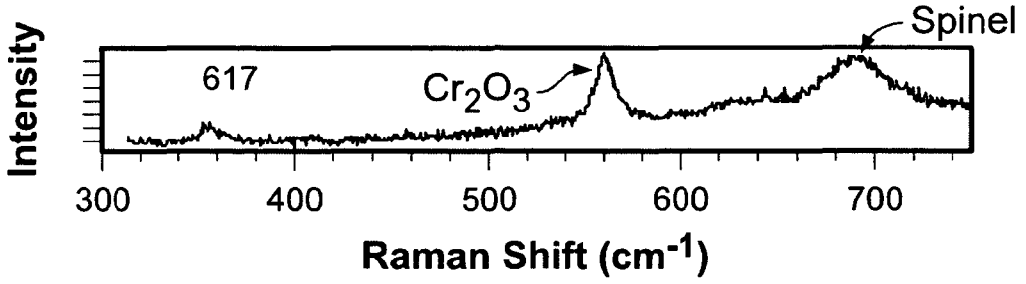

FIG. 25C

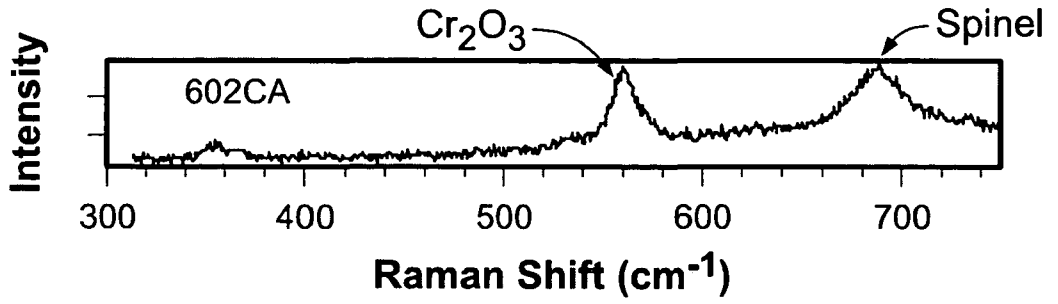

FIG. 25D

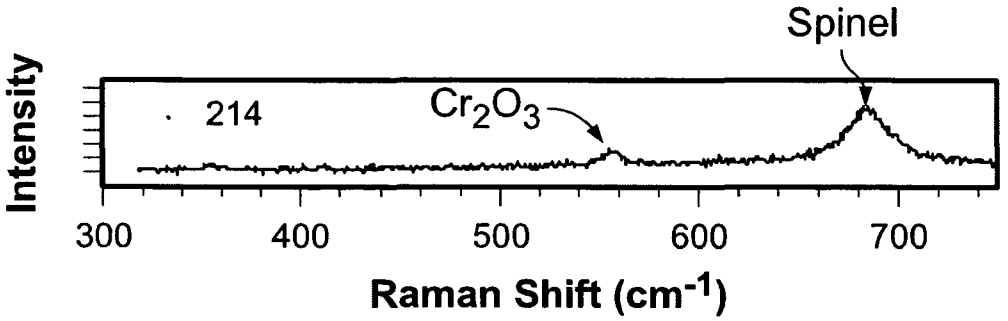

FIG. 25E

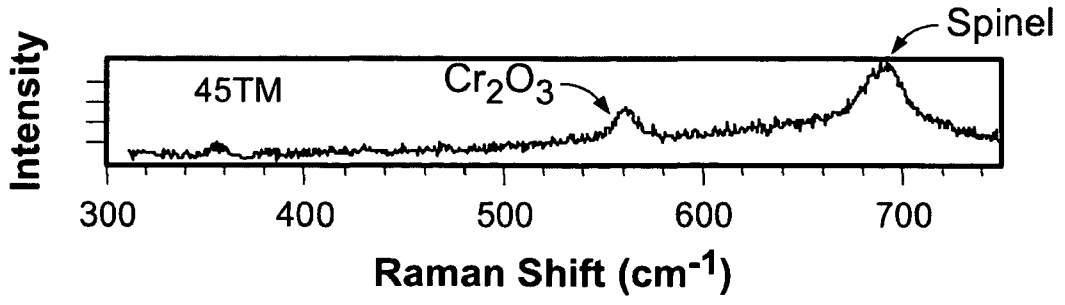

FIG. 25F

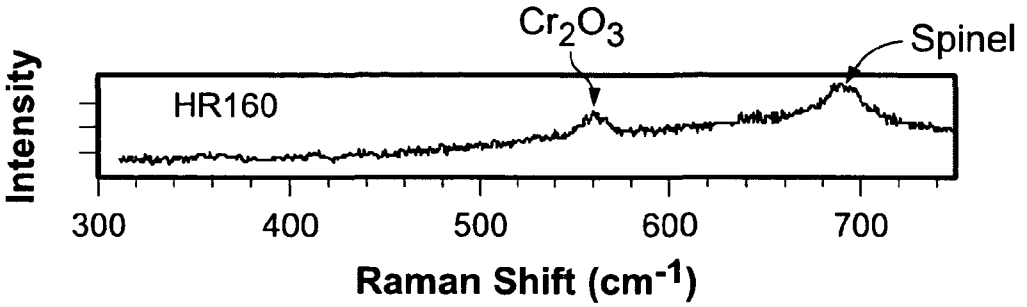

FIG. 25G

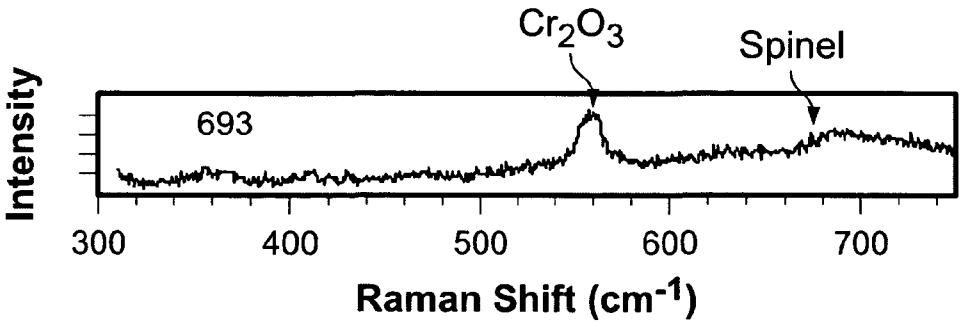

FIG. 25H

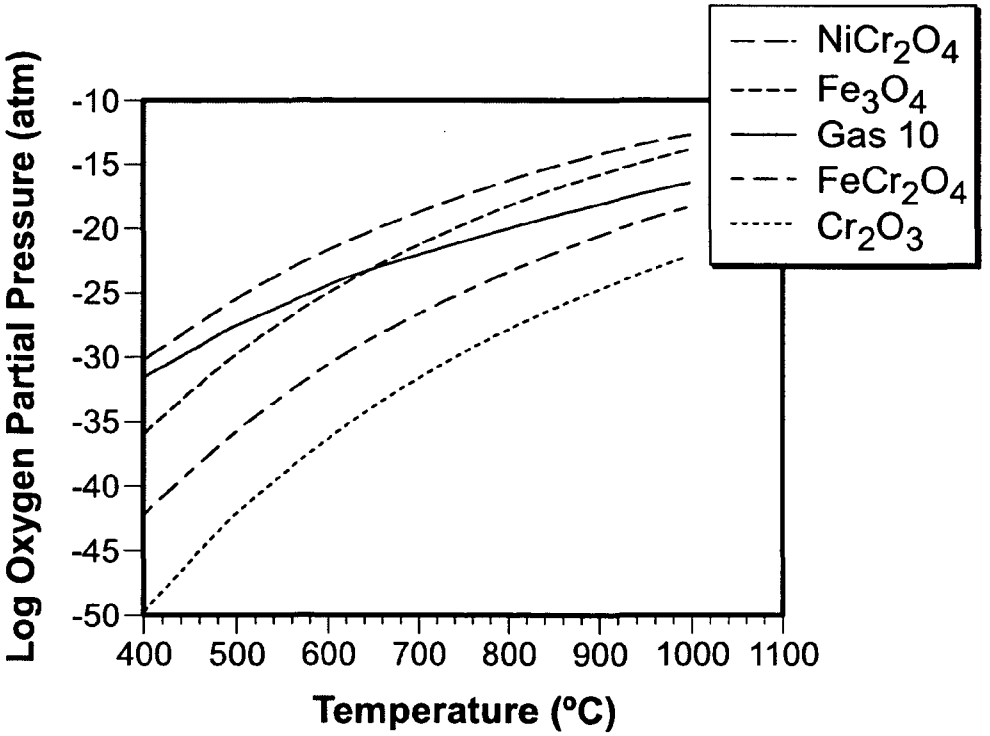

FIG. 26

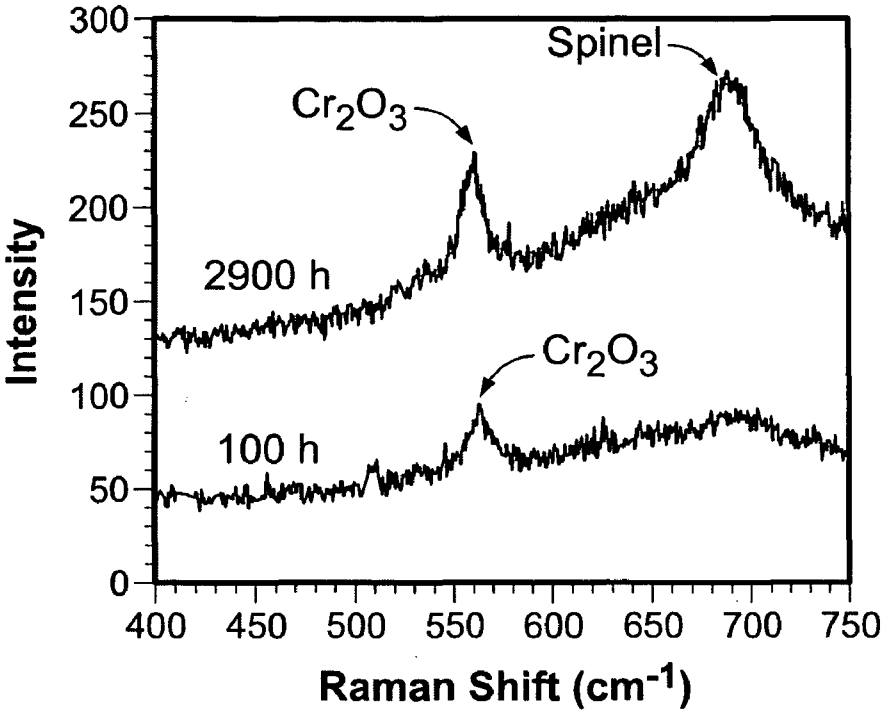

FIG. 27A

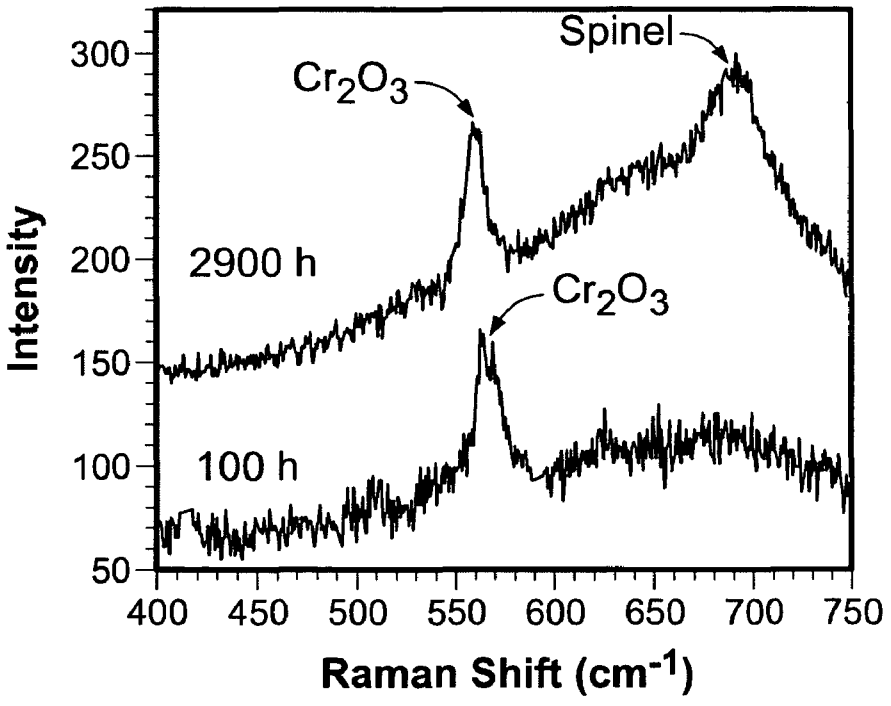

FIG. 27B

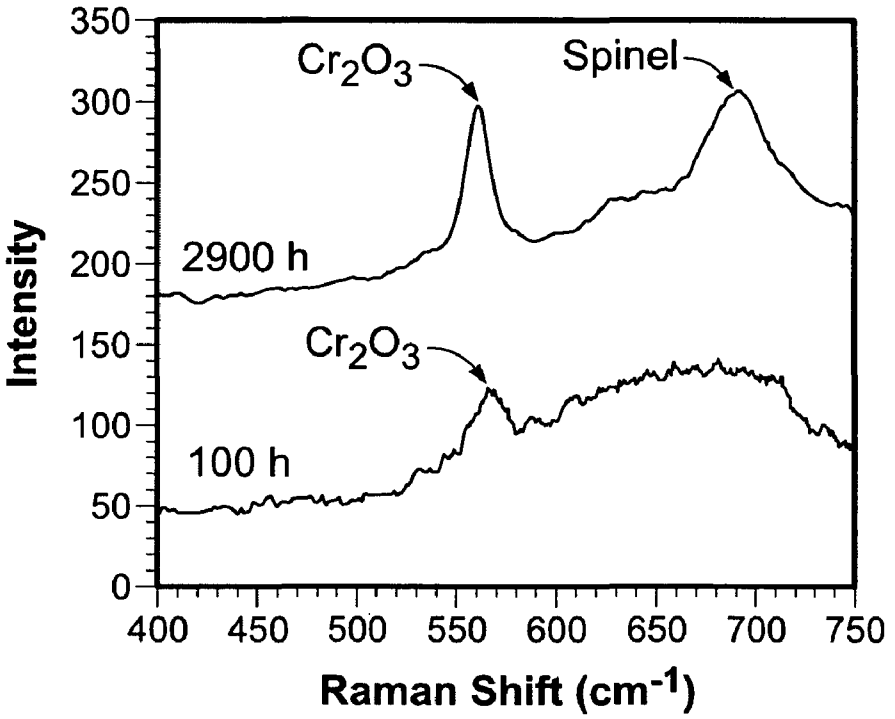

FIG. 27C

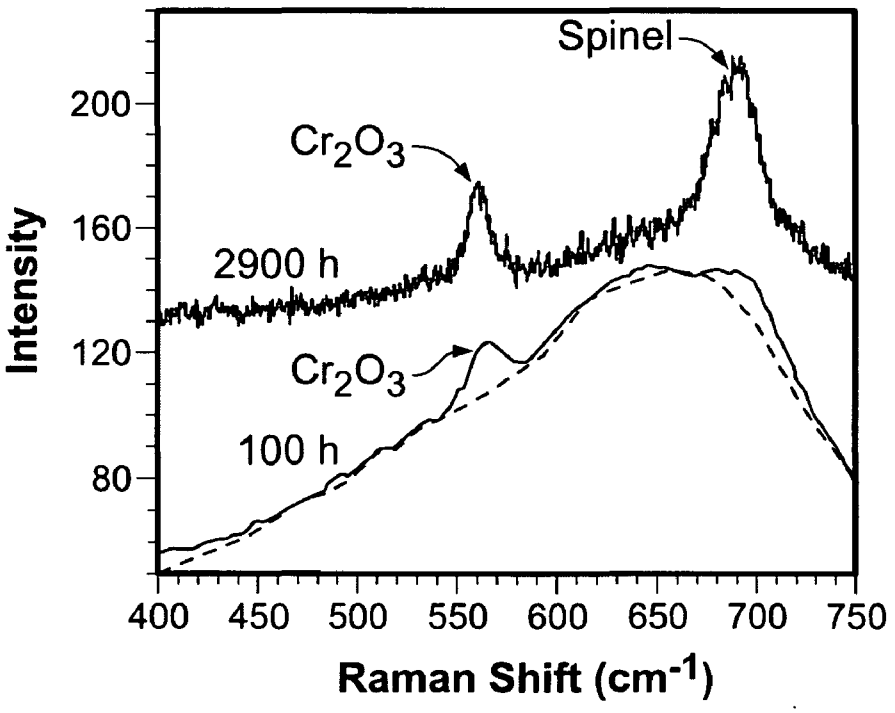

FIG. 27D

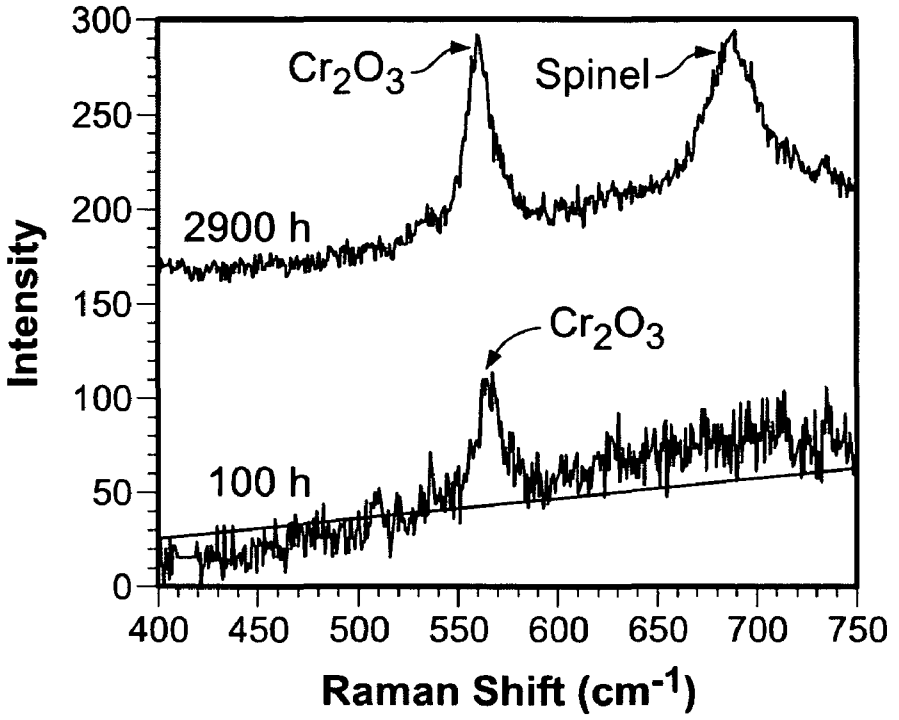

FIG. 27E

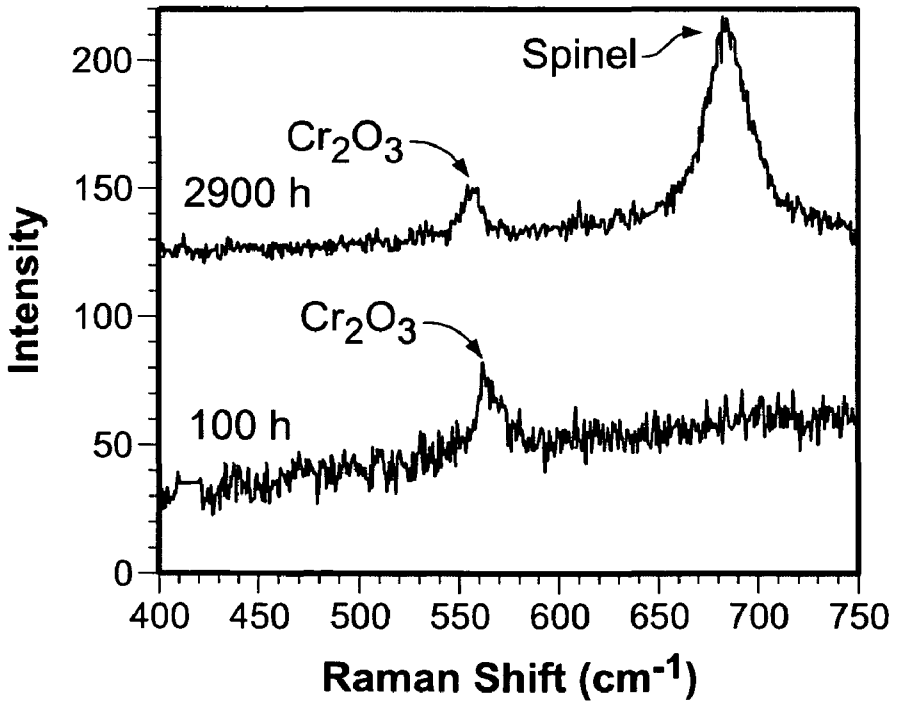

FIG. 27F

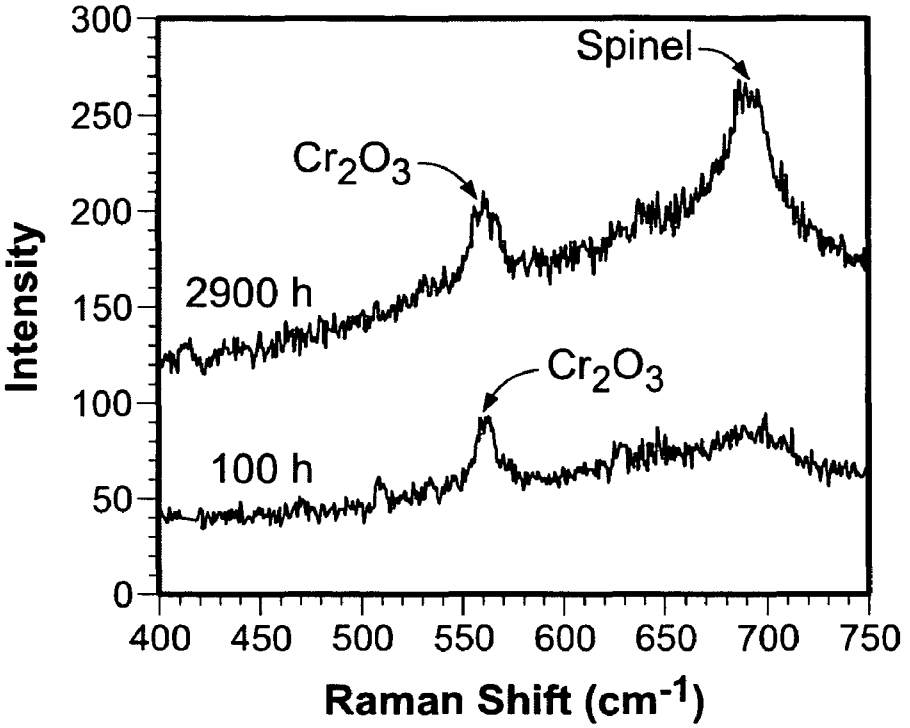

FIG. 27G

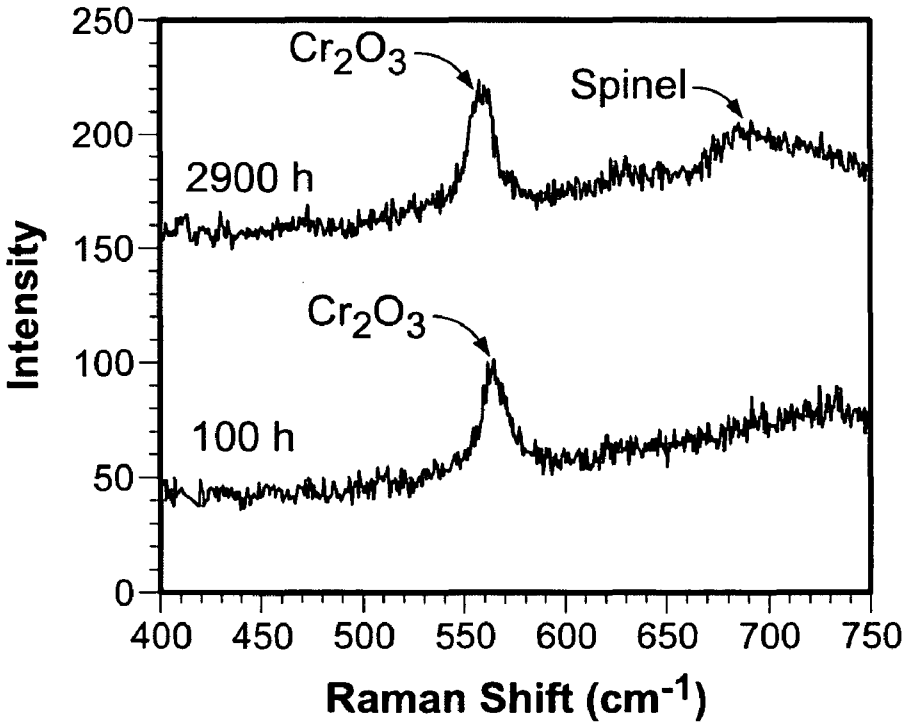

FIG. 27H

NICKEL BASED ALLOYS TO PREVENT METAL DUSTING DEGRADATION

CROSS-REFERENCE TO RELATED PATENT APPLICATIONS

[0001] This application claims the benefit under 35 USC 119(e) of U.S. Application 60/686,480, filed Jun. 1, 2005, incorporated herein by reference in its entirety.

GOVERNMENT INTEREST

[0002] The United States Government has certain rights in the invention pursuant to Contract No. W-31-109-ENG-38 between the U.S. Department of Energy and the University of Chicago operating Argonne National Laboratory.

BACKGROUND OF THE INVENTION

[0003] This invention relates to a method of manufacture and alloy composition for preventing metal dusting degradation. More particularly the invention relates to nickel-based alloys with aluminum addition and also to the use of a copper-based layer to prevent metal dusting-corrosion.

[0004] Metal dusting is a catastrophic corrosion phenomenon that leads to the deterioration of structural metals and alloys into a dust composed of fine particles of the metal/alloy and carbon. This is usually a localized form of attack and occurs at intermediate temperatures of about 350°-800° C. However, this type of corrosion is possible at any temperature when the carbon activity (a_c) in the gas phase is >>1. Metal dusting corrosion occurs in many metallic alloys, particularly Fe-, Co- and Ni-base alloys, when exposed to carbonaceous atmospheres. Under these conditions, the alloys undergoing metal dusting develop pits and holes on the surface, and then disintegrate into a powdery mixture of carbon, oxides, carbides, and fine metal particles. Metal dusting is a more severe problem than carburization since process equipment or component piping will be functionally inoperative from damage occurring when alloys become fine powder.

[0005] Petroleum refineries are one example of industrial environments which need to operate in high carbon activity environments; and as a result, the equipment experiences metal wastage in processes involving hydro-dealkylation and catalyst re-generation systems. Metal wastage also occurs in direct iron-ore reduction plants wherein reformed methane is dried and reheated to enhance ore-reduction efficiency. The ammonia synthesis process also shows metal wastage in the heat-recovery section of the reformed-gas system as well as in the reformer itself. Gases used in heat-treating mixtures contain oil residue on items to form gases that are chemically favorable for metal dusting. Gas mixtures used for carburizing can also cause metal wastage if control of chemistry is not managed. Therefore, the heat-treat industry also suffers metal wastage problem. Other example processes wherein metal wastage occurs are nuclear plants that employ carbon dioxide for cooling the recycle gas loop equipment of coal-gasification units, iron-making blast furnaces in steel mills, and fuel cells that use hydrocarbons.

[0006] Metal dusting usually occurs at temperatures as low as 350° to about 800° C. In a hydrogen plant, hot carbon bearing gases are produced primarily by steam reforming and partial oxidation of hydrocarbon at temperatures of 800-1000° C. These gases have to be quenched to 300° C. to avoid metal dusting in the temperature window 400-800° C. Energy in high temperature syngas is not recovered in an efficient manner. Plant production is generally affected by unforeseen shut-downs due to metal wastage problem. Therefore, it is necessary to develop new methods to prevent this metal dusting problem in the temperature window from about 350° to 800° C.

[0007] There are conventional techniques to try to reduce metal dusting by coating construction materials with thin layers of copper which are described in US005676821A. The coatings, in general, contain microporosity which can enable the reactive gases to permeate and degrade the integrity of the thin coating layers. It has been shown that carburizing gas can slowly diffuse through the coating layer and eventually lead to failure of the protective coating. This simple coating approach, even though beneficial in short term, is generally not amenable to prevent metal dusting over long term in the service of metallic structures in process plants.

[0008] Oxide scales also can play a role in preventing alloys from metal dusting corrosion since carbon diffuses much more slowly through the oxide layers, especially if defects such as pores and cracks are not present in the oxide layers. Because oxide scales are potentially useful in preventing metal dusting corrosion, it is important to consider further the role of their composition and microstructural characteristics in the initiation and propagation of metal dusting. However, the composition and phases present in oxide scales have been rarely investigated and thus not well understood since the oxide layer, generally, is too thin to detect and analyze by conventional X-ray methods.

[0009] Copper-aluminum, copper-silicon alloys are also proposed as construction materials to resist metal dusting corrosion (see, for example, WO03072836). However, the mechanical strength of these materials are too low at high temperature for their use as monolithic structural materials for long term service. Many industrial processes involve high pressures and elevated temperatures. Therefore, new approaches are needed to resist metal dusting corrosion of metallic structures for service at high temperatures and high pressures over long term periods of interest in the industrial sector.

SUMMARY OF THE INVENTION

[0010] While not meant to limit the scope of the invention, it is believed that metal dusting is due to the crystallization of carbon inside the substrate alloys. Carbon diffuses into alloys after it deposits on a surface by catalytic reaction of the gas phase constituents. Carbon then finds a special facet of microcrystal in a metal and precipitates inside the metal, and this process leads to the separation of metal particles. The bulk alloy then finally separates into fine particles and/or metal dust. Whenever carbon diffuses into the alloy, metal dusting is difficult to stop, and an effective way to prevent metal dusting is to build a dense barrier on a surface of metal and minimize carbon diffusion. If carbon cannot diffuse through the barrier, metal dusting corrosion, generally, does not happen. Usually, alloys develop an oxide scale on its surface to prevent metal dusting, and the diffusion rate of carbon in oxide is very low. However, carbon atoms still

can diffuse through the defects in oxide scale and reduce the Fe-containing spinel phase to form channels for carbon diffusion. Whenever the channels form, there is no way to stop the diffusion of carbon into alloys. This process leads to initiation and propagation of pitting corrosion.

[0011] Copper specimens have been tested in several forms by exposing them in a metal dusting environment at various temperatures. Copper was found to be noncatalytic for carbon deposition. Almost no deposit of carbon was observed in these experiments. The copper was also combined with another metal/metal alloy layer to form a bimetallic barrier layer combination.

[0012] The solubility and diffusion rate of carbon in copper are low. Therefore, copper is an excellent material to prevent metal dusting. However, the mechanical strength of copper at high temperature is too low. It is thus difficult to directly use pure copper as a structural material at elevated temperatures. Most of the materials used in metal dusting environment are in the form of vessels, tubing, and piping. Therefore, bimetallic tubing was prepared with an inner copper tubing and an outer Fe or Ni-base alloy tubing to prevent metal dusting corrosion. This dense copper layer on the inside diameter stops the formation/deposit of carbon and also stops the diffusion of carbon, thereby preventing the outer alloy tube from metal dusting corrosion.

[0013] The present invention also relates to several Ni-base alloys as materials for use to provide superior resistance to metal dusting degradation when exposed to highly carbonaceous gaseous environments that are prevalent in hydrogen-, methanol-, and ammonia-reformers and in syngas plants. In addition, the alloys developed have adequate strength properties for use as monolithic structural materials in the chemical, petrochemical, and syngas plants at temperatures up to 900° C. The alloys developed have composition ranges (in wt. %) as follows: C 0.02-0.2, Cr 22-29, Al 2.3-3.3, Fe 0-1, Ti 0.3, Zr 0.1-0.2, Y 0-0.1, Balance Ni (all ranges are approximate). The Ti, Zr and C additions are made to control the carbide precipitation and thereby improve the mechanical strength properties at elevated temperatures. Zr and Y additions also contribute to improve the adhesion of the oxide scale to the substrate alloy. The Cr and Al additions in the alloy greatly assist in resisting metal dusting.

BRIEF DESCRIPTION OF THE DRAWINGS

[0014] FIG. **1** illustrates a schematic drawing of a cross section of a bimetal (Cu/Fe or Ni based alloy) tubing;

[0015] FIG. **2**A illustrates alloy 800 after exposure in a carburizing gas for 3700 h and FIG. **2**B illustrates alloy 321 after exposure in a carburizing gas for 3700 h;

[0016] FIG. **3** illustrates a 3D-profile mapping of corrosion pits in alloy 800 tested in a metal dusting environment at 593° C. for 150 h;

[0017] FIG. **4** illustrates an SEM image of Type 321 stainless steel tested in a metal dusting environment at 593° C. for 1100 h;

[0018] FIG. **5**A illustrates an iron specimen with a 0.8 mm Cu-cladding tested in a metal dusting environment at 593° C. for 600 h, and FIG. **5**B illustrates a base iron coupon tested under the same conditions as the specimen of FIG. **5**A;

[0019] FIG. **6** illustrates weight change data for copper and iron based alloys after exposure in Gas No. 11 at 593° C. and 1 atmosphere pressure;

[0020] FIG. **7** illustrates copper and nickel based alloys exposed to Gas No. 14 at 593° C. at 1 atmosphere pressure;

[0021] FIG. **8** illustrates Raman shift versus intensity for a simulated fit of a broad band for Alloy 153MA with Cr_2O_3 and spinel Raman bands superimposed on the broad band;

[0022] FIG. **9** illustrates weight change data for various (Fe, Cr) spinel phases and (Ni, Cr) spinel phase during exposure in a metal dusting gas mixture at 593° C.;

[0023] FIG. **10** illustrates X-ray diffraction data for $FeCr_2O_4$ and other oxides for Alloy 800 after exposure in a carburizing gas consisting of vol. %: 66.2H_2-7.1 CO_2-23 CO-1.4 CH_4-2.3H_2O at 593° C. for 1000 h;

[0024] FIGS. **11**A-**11**D illustrate Raman data for different Alloys 253MA, 153MA, T91 and T22 after exposure in a carbonizing gas consisting of vol. %: 52H_2-5.6 CO_2-18 CO-1.1 CH_4-23H_2O at 593° C. for 1000 h;

[0025] FIG. **12** illustrates Raman spectra of Alloys 253MA and 601;

[0026] FIG. **13** illustrates Raman spectra of Alloys 310 and 602CA;

[0027] FIG. **14** illustrates Raman spectra of Alloy 601 exposed in a carburizing gas consisting of vol. %: 53.4H_2-18.4 CO-5.7 CO_2-22.5H_2O at 593° C. at 200 psi for 100 and 2900 h;

[0028] FIG. **15** illustrates Raman spectra of Alloy 690 exposed in a carburizing gas consisting of vol. %: 53.4H_2-18.4 CO-5.7 CO_2-22.5H_2O at 593° C. at 200 psi for 100 and 2900 h;

[0029] FIG. **16** illustrates Raman spectra of Alloy 45™ exposed in a carburizing gas consisting of vol. %: 53.4H_2-18.4 CO-5.7 CO_2-22.5H_2O at 593° C. at 200 psi for 100 and 2900 h;

[0030] FIG. **17** illustrates thermal stability of spinel and Cr_2O_3 phases in Gas **10** consisting of (in vol %) 53.5H_2-18.4 CO-5.7 CO_2-22.5H_2O.

[0031] FIG. **18**A illustrates schematically a mechanism for diffusion of carbon and metal dusting of an alloy without presence of Al in the alloy and FIG. **18**B with the presence of Al in the alloy;

[0032] FIG. **19** illustrates a schematic of a high pressure, high temperature test facility;

[0033] FIG. **20**A illustrates an SEM micrograph of Alloy 601 after exposure to a metal dusting environment at 14.3 atmosphere and 593° C. for 160 h; FIG. **20**B is Alloy 601 at 1 atmosphere and 593° C. for 240 h; FIG. **20**C is for Alloy 690 at 14.3 atmosphere and 593° C. for 160 h; FIG. **20**D is for Alloy 690 at 1 atmosphere at 593° C. for 240 h; FIG. **20**E is for Alloy 617 for 14.3 atmosphere and 593° C. for 160 h; FIG. **20**F is alloy 617 at 1 atmosphere and 593° C. is for 240 h; FIG. **20**G is for Alloy 214 at 14.3 atmosphere and 593° C. for 160 h; and FIG. **20**H is for Alloy 214 at 1 atmosphere and 593° C. for 240 h;

[0034] FIG. **21** illustrates weight loss data for several Ni-based alloys (see inset lists of alloys) after exposure in a metal dusting environment at 593° C. and 14.3 atmosphere;

[0035] FIG. **22**A illustrates an SEM micrograph of Alloy 45™ showing pit size variation after 1540 h; with FIG. **22**B after 2180 h; FIG. **22**C after 2500 h; and FIG. **22**D after 3300 h; FIG. **22**E is for alloy 690 after 2900 h; with FIG. **22**F after 4100 h; FIG. **22**G after 7300 h and FIG. **22**H after 9300 h; FIG. **22**I is for alloy 617 after 2900 h; with FIG. J after 4100 h; FIG. **22**K after 7300 h and FIG. **22**L after 9300 h;

[0036] FIGS. **23**A-**23**G illustrate correlation of weight loss and variation in corrosion pit size for a single pit on the surface of the indicated alloy series as a function of exposure time at 593° C. in a metal dusting environment;

[0037] FIGS. **24**A-**24**H illustrate 3D-profile mapping of the surface of the indicated Ni-based series of alloys after 9700 h exposure in a metal dusting environment at 593° C. and 14.3 atmospheres;

[0038] FIGS. **25**A-**25**H illustrate Raman spectra for the indicated Ni-based series of alloys after 2900 h exposure in a metal dusting environment at 593° C. and 14.3 atmosphere;

[0039] FIG. **26** illustrates thermal stability of various indicated spinel and Cr_2O_3 phases; and

[0040] FIG. **27**A illustrates Raman spectra of Alloy N06601 after exposure for 100 h and 2900 h for 593° C. in a metal dusting environment at 593° C., FIG. **27**B for N07790, FIG. **27**C for 617, FIG. **27**D for 45™, FIG. **27**E for 625; FIG. **27**F for 214; FIG. **27**G for HR160 and FIG. **27**H for 693.

DETAILED DESCRIPTION OF THE PREFERRED EMBODIMENTS

Multi-Layer Metal Tubing

[0041] In a first embodiment of the invention a multi-layer metal tubing is illustrated schematically in FIG. **1** at **10**. The most preferred form of the invention constitutes a bi-metal Cu/Fe or Ni based alloy. The thickness of copper and copper alloy tubing is >0.1 mm. It can be preferably bonded or fabricated without bonding between copper inner tubing **12** and outer alloy tubing **14**. Bonding is better because carburizing gas cannot diffuse through between the two tubes in case there is a defect in the copper tubing **12**. To bond the copper tubing **12** together, a thin layer of low melting temperature metals or their mixtures such as zinc, silver, tin, and cadmium, were coated either on outer surface of the copper tubing **12**, or on the inner surface of the alloy tubing **14**, or both surfaces. High temperature and pressure were applied to bond the tubes together.

[0042] Experiments were conducted in a horizontal furnace with a quartz tube (2 in dia.) at 1 atm and in a tube furnace at high pressures. The test temperature was 593° C. (1100° F.). The experiments are conducted in several gas mixtures and at several system pressures. Some samples were tested for >10000 h. The composition of test gases used for the evaluation is shown in Table 1.

TABLE 1

Chemical compositions of gas mixture relevant for metal dusting study.

Gas	H_2 (mol %)	C_O (mol %)	$C0_2$ (mol %)	H_20 (mol %)	CH_4 (mol %)	Other (mol %)
1	43.8	7.2	5.7	39.2	4.1	—
2	52	18	5.6	23	1.1	—
2b	66.2	23	7.1	2.3	1.4	—
3	36.3	8.4	5.6	35	0.2	N_2 15, Ar 0.1
4	74.2	17.5	8.3	0	—	—
5	72.2	17.6	8.3	2.0	—	—
6	77.2	12.7	10.1	0	—	—
7	25.3	70	4	0.01	—	—
8	71.4	11.3	17.4	0	—	—
9	71	11.7	17.3	0	—	—
10	53.4	18.4	5.7	22.5	—	—
11	79.5	18.2	—	2.3	—	—
12	75.4	6.2	18.4	—	—	—
13	71.0	2.6	26.4	—	—	—
14	40	45	5	10	—	—
15	20	65	5	10	—	—
16	40	25	25	10	—	—
17	20	74.5	5	0.5	—	—

[0043] Table 2 shows that copper and copper alloy specimens were resistant to degradation by metal dusting. However, most of the state-of-the-art, commercial and experimental Fe- and Ni-base alloys were attacked in the same environment. FIGS. **2** and **3** shows pits that were observed on surfaces of Alloys 800 and 321 stainless steel after exposure in metal dusting environment. FIG. **4** shows that a deep pit that developed in Alloy 321. In Alloy 800, carbon was heavily deposited on the surface and metal dusting pits were observed, whereas, carbon neither was visually observed on the copper sample, nor was detected by X-ray diffraction. This indicates that copper did not catalyze the gas phase reaction to deposit carbon. Therefore, the carbon growth rate on copper was extremely low.

[0044] FIG. **5**A shows the surface of the copper-clad iron specimen after exposure to metal dusting environment at 593° C. The surface was clean and devoid of any deposit of carbon. The clad specimen did not lose weight after metal dusting test. However, the surface of the bare (un-clad) iron specimen of FIG. **5**B was covered by carbon after metal dusting exposure for only 100 h iron was consumed at a rate of 0.55-mg/cm^2-h. The test results indicate that application of a dense copper clad >0.1 mm on the alloy surface prevented metal dusting attack.

[0045] FIG. **6** shows a series of metals and metal alloys (alloy key in the inset box). FIG. **6** indicates copper was not attacked by metal dusting even after exposure for >7000 h. However, other Fe-base alloys lost weight significantly during the same exposure period. Copper alloys also showed strong resistance to metal dusting. No weight losses were observed for these alloys after 3000 h exposure to carburizing gas. Meanwhile, Ni-base Alloy 214 severely lost weight (see FIG. **7**).

TABLE 2

Metal dusting experimental results for Cu alloys

Exp. #	Material	Gas #	Time (h)	Pressure (atm)	Results
33	Cu coated iron and alloys	4	163	1	Clean surface
35	Cu clad Fe plate	4	784	1	Clean surface
36	Glidcop	4	144	1	Clean surface
37	Cu coated iron and alloys	4	120	1	Clean surface
41	Cu	8	100	27	Clean surface
42	Cu	8	100	14	Clears surface
43	Cu	13	100	41	Clean surface
45	Glidcop	4	300	1	Clean surface
49	Cu	10	1131	14	Clean surface
50	Cu	10	100	14	Clean surface
51	Cu	10	113	41	Clean surface
52	Cu	10	680	41	Clean surface
53	Cu	11	8348	1	Clean surface
54	Cu	14	1950	1	Clean surface
56	Cu—Ni-A1 2	14	10027	1	No weight loss
56	Cu—Ni-A1 4	14	10027	1	No weight loss
56	Cu—Ni-AI 12	14	10027	1	No weight loss
56	Cu—Ni-A1 20	14	10027	1	No weight loss
59	Cu—Ni-A1 2	10	8900	14	No weight loss
59	Cu—Ni-A1 4	10	8900	14	No weight loss
60	Cu	10	246	1	Clean surface

B.—Nickel-base Alloys with Low Iron Content

[0046] Extensive studies were conducted on metal dusting with a variety of commercial Fe- and Ni-base structural alloys in environments that simulate reformer environment. Alloys generally develop oxide scales in the exposure environment, but depending on the phases present in the oxide scales in the reduction of these phases, lead to nucleation and growth of pits leading to catastrophic failure of the alloy into powder. The characteristics of different oxide scales were examined and also correlated the information with the compositions of the alloys and their resistance to metal dusting.

[0047] It was determined that diffusion of carbon through oxide scale is difficult. However, Fe-, Co, and Ni-base alloys cannot avoid metal dusting corrosion if high activity carbon diffuses into the alloys. Therefore, the quality of the oxide scale is very important for alloys to resist metal dusting corrosion. Raman experiments show there are three types of oxides in oxide scale, which are Cr_2O_3, disordered chromium oxide, and $Fe_{1+x}Cr_{2-x}O_4$ ($0 \leqq x \leqq 1$) spinel (FIG. **8**).

[0048] To study the reaction of these oxides with carburizing gas, Cr_2O_3, $(Fe, Cr)_3O_4$ spinel, and Cr metal were tested in a carburizing gas consisting of (in vol. %) $52H_2$-5.6 CO_2-18CO-1.1CH_4-23H_2O at 593° C. in a thermo gravimetric test apparatus. Disordered chromium oxide and Cr_2O_3 formed on the surface of Cr metal. Weight gains of $FeCr_2O_4$, Cr_2O_3, and Cr metal were almost zero. Although the carbon activity of the carburizing gas consisting of (in vol. %) $52H_2$-5.6CO_2-18CO-1.1CH_4-23H_2O was >1 at 593° C., the deposition of carbon on Cr_2O_3, disordered chromium oxide, and $FeCr_2O_4$ is difficult since the activation barrier is high for the following reactions:

$$CO+H_2=C+H_2O \quad (1)$$

$$2CO=C+CO_2 \quad (2)$$

[0049] If the alloy surface is totally covered by Cr_2O_3, disordered chromium oxide, and $FeCr_2O_4$, carbon deposition and metal dusting may not occur. However, weight gain was observed for $Fe_{1.8}Cr_{1.2}O_4$, and the carbon deposition rate in $Fe_{2.4}Cr_{0.6}O_4$ was much larger than that of $Fe_{1.8}Cr_{1.2}O_4$ (FIG. **9**). Therefore, spinel with high iron content seems to catalyze reaction **1** and/or **2**, which leads to deposition of carbon.

[0050] Cr_2O_3 is stable in carbon and hydrogen atmospheres down to very low Po_2. This oxide is an excellent protective layer in preventing alloys from metal dusting corrosion. $Fe(Cr_{1-x}Fe_x)_2O_4$ spine, on the other hand, is not as stable as Cr_2O_3. The composition of the spinal can vary from $FeCr_2O_4$ [x=0 in $Fe(Cr_{1-x}Fe_x)_2O_4$] to Fe_3O_4 (x=1). As mentioned above, Fe_3O_4 is not stable when the H_2O concentration is low. The stability of $FeCr_2O_4$ is higher than that of Fe_3O_4, but lower than that of Cr_2O_3. If there are no defects such as nonuniform distribution of cations, $FeCr_2O_4$ should be stable in a carburizing gas. However, it has been reported that $FeCr_2O_4$ starts to be partially reduced by carbon at 600° C. FIG. **10** shows that the X-ray peak position of the spinal on the surface of Alloy 800 is between Fe_3O_4 and $FeCr_2O_4$, and the peak is also much broader than that of polycrystalline Fe_3O_4 and $FeCr_2O_4$. Thus, it appears the spinal on the surface of alloy is not stoichiometric $FeCr_2O_4$, but has higher iron content and such a spine is likely susceptible to reduction by carbon.

[0051] The higher the concentration of iron in $Fe(Cr_{1-x}Fe_x)_2O_4$, the easier is the spinel reduction. The ratio of Fe/Cr in spinel may vary with oxygen partial pressure in gas. When Po_2 in gas, such as in Gas **1**, is higher than 7×10^{-26} atm, the most unstable spinel Fe_3O_4 could form, which could be attacked by carbon leading to metal dusting corrosion of the underlying alloy. It is difficult to measure the iron content in the oxide layer because it is too thin. However, the iron content in the oxide scale increases with increasing iron content in the alloy. Furthermore, the iron concentration may not be uniform in the oxide scale. Some spots with high iron content may react with carbon first and metal dusting will start from those regions. FIG. **11**B shows that alloy 153MA has less spinel phase in the oxide scale than does T91; therefore, 153MA has fewer defects susceptible to attack by metal dusting corrosion than does alloy T91 of FIG. **11**C. This is also consistent with the observation of smaller mass loss for 153MA than that for T91.

[0052] FIGS. **12** and **13** show the differences in Raman spectra for two pairs of alloys: Alloy 253MA and 601, and Alloy 310 and 602CA. These alloys were exposed for 1000 h to Gas **10** at 593° C. and 200 psi. The Cr content in Alloy 253MA (20.9%) and 601 (21.9%) is similar. However, the Fe-base alloy 253MA has a much stronger spinel peak than that of the Ni-base alloy 601 (FIG. **12**). Pits were observed on Alloy 253MA, but not on Alloy 601 when exposed under the same experimental conditions. The Cr content in Alloy 310 (25.5%) and 602CA (25.1%) is also similar. FIG. **13** shows the strong spinel peak for the Fe-base Alloy 310, but almost no such peak for the Ni-base Alloy 602CA. Pits were again observed only on Alloy 310, but not on Alloy 602CA. Less spinel in the oxide scale of Ni-base alloys only means that the development of spinal takes a much longer time and that the incubation time for metal dusting initiation is much longer. However, the presence of Fe, even in low concentration, in Ni-base alloys will lead to metal dusting degradation during years of service planned for these structural components in reformer environments.

[0053] Phase composition of oxide scales that developed on surface of alloys changes with exposure time. FIGS. **14** to **16** (601, 690, 45™) show the intensity differences of Raman bands for Cr_2O_3 and spinel phases in oxide scale on surfaces of several alloys. When the alloys were exposed for only 100 h, Cr_2O_3 was the major phase in oxide scales that developed on surface of alloys. However, after 2900 h exposure, the intensity of spinel band in Raman spectra increased significantly.

[0054] The increasing amount of spinel phase in oxide scales over longer exposure time can be attributed to the outward diffusion of Fe from the alloy substrate. At early stages, Cr-rich oxide forms on the surface of alloys. However, as the outward transported Fe is incorporated into the scale, spinel phase becomes dominant as was observed in the Raman spectra. The diffusion rate of Fe and its incorporation in the scale to form the spinel phase would have a pronounced effect on the incubation time for the onset of metal dusting in the alloy. As the transported Fe is incorporated into the spinel phase, the protective capacity of the spinel is reduced, since the inward migrating carbon can easily reduce the high-iron-containing spinel (as discussed earlier).

[0055] Raman spectra showed that the intensity of Cr_2O_3 band at ≈560 cm^{-1} was low for Alloy 45™ and the relative intensity of spinel is high. As was discussed earlier, spinal phase in the scale is not as good as Cr_2O_3 scale in preventing alloys from metal dusting corrosion, which probably is the cause for the alloy to undergo metal dusting. The Cr content in 45™ is relatively high but the Fe content is also high. The presence of high Fe content may stabilize the Fe-containing spinal phase rather than Cr_2O_3, thereby subjecting the alloy to metal dust. $NiCr_2O_4$ spine is not thermodynamically stable in a reducing environment used in our study and therefore, could not form at 593° C. (see FIG. **17**). The results suggest that an alloy with a high Cr content (with or without Al) and almost no Fe content may stabilize Cr_2O_3 and/or a spinal phase with high Cr content, thereby prolong the incubation period for the onset of metal dusting and subsequent propagation of the process leading to metal wastage. Even small addition of iron will affect the quality of oxide scale and decrease the ability of alloys to resist metal dusting.

[0056] FIGS. **18**A and **18**B are schematic representations of a non-limiting mechanism that explains the function of aluminum in the resistance of alloys to metal dusting corrosion. Physical defects may be present in oxide scales that develop on the surface of alloys. When carbon deposits on these surfaces during exposure to a metal dusting environment, carbon diffuses through these defects and reduces the spinel phase to Fe_3C and/or Ni metal. These particles form channels for transferring carbon through the oxide scale. Oxygen may also diffuse through these channels leading to the formation of additional Cr oxide and slowing the diffusion of carbon. However, the carbon diffusion rate is probably higher than that of oxygen and formation of additional Cr oxide beneath the carbon channel may not be feasible. Therefore, carbon can continue to diffuse into alloys through the channels and finally form metal dusting pits. When Al is added to the alloy, alumina scale usually forms under the Cr oxide scale. The alumina may affect resistance to metal dusting corrosion in two ways. First, the carbon transferred through the channel may not be able to penetrate through the alumina layer because alumina is much more stable than spinel. Second, the partial pressure of oxygen needed to form Al_2O_3 (3.6×10^{-57} atm) is much lower than that needed to form Cr_2O_3 (2.6×10^{-37} atm) at 593° C. A thin layer of alumina scale can form (even with limited oxygen transport through the channel) beneath the carbon diffusion channel, and thereby reduce the growth of metal dusting pits.

[0057] Various non-limiting examples are provided hereinafter and are based on the following experimental procedure:

EXAMPLES

[0058] The test program included eight Ni-base wrought alloys, predominantly those which are commercially available. Table 3 lists the nominal chemical compositions of the alloys. The alloys had complex chemical compositions and contained Cr (in a range of 15.4-28 wt. %) and several other elements, such as Mo [alloy 617 (UNS N06617)], Al [601 (UNS N06601), 617 (UNS N06617), 602CA (UNS N06025), 214 (UNS N07214), and 693 (UNS N06693)], and Si [45™ (UNS N06045) and HR 160 (UNS N12160)]. Alloy 690 (UNS N06690) containing 27.2 wt. % Cr, but without additions of Si, or Mo, or Al was also included in the study. Further, several alloys contained Nb, W, and Co, which can also influence the oxidation behavior of the alloys and their resistance to metal dusting attack.

TABLE 3

Nominal composition (in wt. %) of alloys selected for the study.

Alloy UNS.	C	Cr	Ni	Mn	Si	Mo	Al	Fe	Other
N06601	0.03	21.9	61.8	0.2	0.2	0.1	1.4	14.5	Ti 0.3, Nb 0.1
N06690	0.01	27.2	61.4	0.2	0.1	0.1	0.2	10.2	Ti 0.3
N06617	0.08	21.6	53.6	0.1	0.1	9.5	1.2	0.9	Co 12.5, Ti 0.3
N06025	0.19	25.1	62.6	0.1	0.1	—	2.3	9.3	Ti 0.13, Zr 0.19, Y 0.1
N07214	0.04	15.9	Bal	0.2	0.1	0.5	3.7	2.5	Zr 0.01, Y 0.006
N06045	0.08	27.4	46.4	0.4	2.7	—	—	26.7	RE 0.07
N12160	0.05	28.0	Bal	0.5	2.8	0.1	0.2	4.0	Co 30.0
N06693	0.02	28.8	Bal	0.2	—	0.1	3.3	5.8	Nb 0.7, Ti 0.4, Zr 0.03

[0059] The samples were flat coupons with approximate dimensions of 12×20×1 to 2 mm. They were sheared slightly oversize, and their edges were milled to remove cut edges and reduce the coupons to final size. A standard surface finish was used for all alloy specimens. The finish involved a final wet grinding with 400-grit SiC paper. Stenciling or electric engraving at the corner of the coupons identified all of the specimens. Prior to testing, specimens were thoroughly degreased in clean acetone, rinsed in water, and dried. The specimen dimensions were measured to ±0.02 mm, and the total exposed surface area, including edges, was calculated. The specimens were weighed to an accuracy of 0.1 mg.

[0060] FIG. **19** shows a schematic of a system that was used to conduct experiments at system pressures up to 600 psi. The system consisted of a horizontal, tubular, high temperature furnace capable of operation up to 900° C. The

reaction chamber, with gas inlet/outlet fittings, fabricated from alumina and/or quartz was positioned within a pressure vessel made of a high temperature heat-resistant alloy (16-mm ID, 50-mm OD, 500-mm long). A chromel-alumel thermocouple was inserted into the pressure vessel to monitor the specimen temperature. Specimens were suspended from a quartz specimen holder and were positioned in the constant-temperature section of the tubular furnace. High-purity gases such as CO, CO_2, and H_2, were piped into the reaction chamber through flow meters to obtain the desired composition. To include steam in the exposure environment, water was pumped from a water pump, converted to steam, pressurized, and inserted along with the gas mixture. The effluent from the reactor chamber was condensed to remove the water prior to exhaust. Specimens were exposed to a flowing gas consisting of 53.4% H_2-5.7% CO_2-18.4% CO-22.5% H_2O at 593° C. and 14.3 atm. The gas is a simulation of a reformer outlet gas. The calculated carbon activity of the gas at 593° C. is 2.2, 31, and 89 at 1, 14.3 and 40.8 atm, respectively, based on the reaction $CO+H_2=C+H_2O$.

[0061] Several analytical approaches and techniques were used to evaluate the tested specimens. These included metal weight gain/loss in as-exposed and cleaned conditions, pitting size and density (pits per unit area of surface), pit depth (average depth over significant number of pits), and substrate penetration as determined by metallographic examination. After the specimens were weighed in the as-exposed condition, deposits on the specimens were mechanically removed with a soft brush, and the deposit material was analyzed for metal content, if warranted. The brushed specimens were cleaned ultrasonically to remove residual deposits and then washed in water and dried. Subsequently, the specimens were weighed, and the weight gain/loss was noted. The cleaned specimens were examined for surface pits by optical microscopy. This allowed determination of the number of pits present in different regions of the specimen and the pit density. In addition, the sizes of several pits were measured and averaged to establish an average pit size.

[0062] At the end of a given run, several of the cleaned specimens (after weighing and pit measurement) were cut and mounted on the cut faces for metallographic polishing and examination in as-polished and in electrolytically etched (with a 10% acetic acid solution at 10 V for 30 sec) conditions, by optical and/or scanning electron microscopy. Pit depth and substrate penetration thickness were measured in several exposed specimens. Raman spectra were excited with 60 mW of 476-nm radiation from a Kr-ion laser. The incident beam impinged on the sample at an angle=45° from the normal. Scattered radiation was collected along the surface normal with an NA lens and was analyzed with a triple Jobin-Yvon grating spectrometer. All of the spectra were acquired in 300 sec at room temperature.

[0063] Ni-base alloys possess better resistance against metal dusting attack than the Fe-base alloys. Without limiting the invention, the difference in the lattice mismatch in catalytic crystallization of carbon may be one reason. The misfit between Ni lattice to graphite lattice (3.6%) is much higher than that between Fe_3C and graphite (0.28%). Lattice of Fe_3C almost perfectly matches the lattice of graphite. This indicates that carbon atoms moving from lattice of Fe_3C to graphite is easier than that from Ni to graphite. Therefore, the precipitation of carbon on surface of Ni has a higher energy barrier than that on surface of Fe_3C, which leads to lower carbon precipitation rate, smaller crystallite size, and lower metal dusting rate. The observed crystallite size of coke on nickel was smaller than that on iron. This difference suggests that Fe_3C is better than Ni in serving as a template for the catalytic crystallization of carbon, and may explain why the metal dusting rate of Fe and Fe-base alloys is higher than that of Ni and Ni-base alloys. The other factor that can affect metal dusting rate is the chemical and mechanical integrity of the oxide layer that develops on the surface of alloys. In this set of examples, the effect of alloy chemistry and phase composition of oxides on surface of Ni-base alloys on metal dusting rates shown. The information on metal dusting rate of several Ni-base alloys was examined in order to establish the best candidate alloys to resist metal dusting corrosion.

Weight Loss and Pit Development

[0064] No metal dusting attack was observed for Ni-base alloys in relatively short exposure time of 246 h at 1 atm pressure (Table 4). However, pits were observed on Alloys N06601, N06690, N06617, and N07214 when exposed in the same gas at 593° C. and 14.3 atm (see Table 2). Similar results were obtained when specimens were tested at 40.8 atm (Table 4). FIGS. **20**A to **20**H show the surface of several indicated alloys after exposure at 593° C. and 1 and 14.3 atm. The carbon activity in the gas is 14 times higher than at 1 atm, which can decrease the incubation time for the initiation of metal dusting pits the alloy surface.

TABLE 4

Surface characteristics of alloys after 246-h exposure at 593° C.

UNS number of alloy	Surface characteristics after exposure at 1 atm	14.3 atm	40.8 atm
N06601	Clean surface	Pits	Pits
N06690	Clean surface	Pits	Pits
N06617	Clean surface	Pits	Pits
N06025	Clean surface	Clean surface	Clean surface
N07214	Clean surface	Pits	Pits
N06045	Clean surface	Clean surface	Clean surface
N12160	Clean surface	Clean surface	Clean surface

[0065] Metal dusting attack, as measured by weight loss, was observed on all the Ni-base alloys when tested for 9700 h in the same gas environment at 593° C. and 14.3 atm (see FIG. **21**). However, the weight loss rates for Alloys N06693 and N06045 were very low. Both alloys contain Al, have high Cr content, and low amount of Fe. The weight loss rate for Alloy N06045 was the highest among the Ni-base alloys used in the study, although the Cr content in this alloy is fairly high. The iron content in Alloy N06045 is also the highest among these alloys. The weight loss rate of Alloy N06601 was also high. The iron content in Alloy N06601 is the second highest among these alloys. The results indicate that addition of iron to the Ni-base alloys results in substantial decrease in incubation time for the onset of metal dusting. When Fe content in the alloy >10 wt. %, the alloy is readily attacked as evidenced by numerous pits on the exposed surfaces of the alloy specimens. The weight loss rate for cobalt-containing Alloy N06617 is the second highest among these alloys. Mo addition in this alloy did not improve its resistance to metal dusting corrosion. The other cobalt-containing Alloy N12160 also exhibited metal dusting degradation, although it contained 28% Cr. Therefore, Co addition in alloys is also not beneficial in resisting metal dusting. The Cr content in Alloy N07214 is the lowest

among these alloys and its weight loss rate was also high although it contained aluminum. High Cr content in alloys seems essential but not entirely sufficient for preventing metal dusting corrosion in Ni-base alloys.

[0066] Even though weight loss data developed for various alloys are useful in evaluation and ranking of the alloys from their susceptibility to metal dusting attack, such data may indicate the protective capacity of the surface oxide scale and probably represent only an average behavior for the alloy in a given exposure environment and temperature. Since the corrosion damage in the alloy occurs by nucleation of pits on the surface and their growth inward, it is essential to develop an understanding of the morphology of pits (such as pit size, pit distribution, pit depth, etc.) on the alloy surface and of the maximum growth rate of the pits to evaluate the ultimate damage of component failure under a given set of exposure (process) conditions.

[0067] During the course of the 9700 h exposure experiment, the specimens were retrieved periodically and SEM photomicrographs taken of different regions all the specimens to characterize and monitor their growth as a function of exposure time. FIGS. **22**A-**22**C show the SEM photomicrographs of pit development in alloys N06045, N06690, and N06617 after exposure for different times in the metal dusting environment at 593° C. and 14.3 atm.

[0068] The dimension of a single pit (for each alloy) was measured as a function of exposure time and correlated the pit size data with measured weight change for the corresponding alloys. Table 5 lists the maximum pit size and weight loss for various alloys. FIGS. **23**A-**23**G show the measured pit size and weight change for all the alloys used in the present study. The plots, for most of the alloys, indicate a good correlation between the growths in the size of an arbitrarily selected pit on the surface of the alloy with the measured weight change. Furthermore, absolute increase in pit size as a function of exposure time is different for different alloys. For example, the pit size increases from 200 to 450 μm as the exposure time increases from 4000 to 9300 h for Alloy N06601. The corresponding increases for Alloy N06690 are 70 to 200 μm for time increase of 2900 to 9300 h. Similar information for other alloys can be obtained from the curved shown in FIGS. **23**A-**24**G.

TABLE 5

	Maximum pit size and weight loss for alloys after 9,700-h exposure.			
UNS number of alloy	Weight loss (mg/cm^2)	Pit depth (μm)	Pit diameter (μm)	Ratio of pit depth to pit diameter
N06601	19.5	110	450	0.244
N06690	6.5	147	440	0.334
N06617	35.1	201	887	0.227
N06025	2.1	96	374	0.256
N07214	25.6		Uniformly corroded	
N06045[1]	59.1	141	600	0.235
N12160	7.3	13	210	0.062
N06693	0.1	37	99	0.374

[1]The alloy was exposed only for 3,300 h whereas the others were exposed for 9,700 h.

[0069] The behavior of alloy N07214 is somewhat different from that of others, since there is a poor correlation between the size increase of a single pit in this alloy with its weight change. The reason for this poor correlation is because this alloy contains low (15.9 wt. %) concentration of Cr and a high (3.7 wt. %) concentration of Al and develops a large number of small pits. The nucleation and growth of a large number of small pits with low growth rates reflects in the weight change but on the growth rate of an individual pit. The alloy exhibited a uniform coverage after 3000 h exposure and the size of an individual pit could not be measured. Alloy N06045 exhibited an extremely rapid growth rate for the pit (380 to 600 μm during 1400 to 3400 h) and its exposure was terminated after 3800 h. The cause for the rapid increase in pit growth in this alloy can be attributed to higher (26.7 wt. %) Fe content of the alloy. FIGS. **24**A-**24**H show a comparison of SEM photomicrographs of surfaces of several alloys after exposure at 9700 h at 593° C. to the metal dusting environment. It is evident from this figure that Alloy N07214 develops a rough surface, attributed to multitude of small and probably shallow pits.

Phase Composition of Scales

[0070] Raman spectra were excited with 60 mW of 476-nm radiation from a Kr-ion laser. The scattered light was analyzed with a triple Jobin-Yvon grating spectrometer. All of our spectra were acquired in 300 sec at room temperature. Raman spectra were developed on alloys after exposure at 100 and 2900 h. FIGS. **25**A-**25**H shows a comparison of Raman spectra obtained on the indicated alloys after exposure at 2900 h to the metal dusting environment.

[0071] Raman spectra showed that the intensity of Cr_2O_3 band at about 560 cm^{-1} was low for both Alloys N07214 and N06045 and the relative intensity of spinel is high in both the alloys. Spinel phase in the scale is not as good as Cr_2O_3 scale in preventing alloys from metal dusting corrosion, which probably is the cause for these two alloys to undergo metal dusting. The low Cr_2O_3 content on surface of Alloy N07214 may be due to the low Cr content in alloy. On the contrary, Cr content in N06045 is relatively high but the Fe content is also high. The presence of high Fe content may stabilize the Fe-containing spinel phase rather than Cr_2O_3, thereby subjecting the alloy to metal dust. The fit to the broad Raman band for alloy N06045 is due to disordered chromium oxide with oxygen vacancies. $NiCr_2O_4$ spinel is not thermodynamically stable in a reducing environment used in our study and therefore, could not form at 593° C. (FIG. **26**). The results suggest that an alloy with a high Cr content (with or without Al) and low Fe content may stabilize Cr_2O_3 and/or a spinel phase with high Cr content, thereby prolong the incubation period for, the onset of metal dusting and subsequent propagation of the process leading to metal wastage.

[0072] Phase composition of oxide scales that developed on surface of alloys changed with exposure time. FIGS. **27**A-**27**H show the intensity differences of Raman bands for Cr_2O_3 and spinel phases in oxide scale on surfaces of several alloys after 100 and 2900 h exposure. When the alloys were exposed for only 100 h, Cr_2O_3 was the major phase in oxide scales that developed on surface of alloys. However, after 2900 h exposure, the intensity of spinel band in Raman spectra increased significantly. On Alloy N07214, spinel became the major phase after exposure for 2900 h, whereas Cr_2O_3 was the major phase in the oxide scale when the alloy had been exposed for 100 h.

[0073] The increasing amount of spinel phase in oxide scales over longer exposure time can be attributed to the

outward diffusion of Fe from the alloy substrate. At early stages, Cr-rich oxide forms on the surface of alloys. However, as the outward transported Fe gets incorporated into the scale, spinel phase becomes dominant as was observed in the Raman spectra. The diffusion rate of Fe and its incorporation in the scale to form the spinel phase would have a pronounced effect on the incubation time for the onset of metal dusting in the alloy. As the transported Fe gets incorporated into the spinel phase, the protective capacity of the spinel is reduced, since the inward migrating carbon can easily reduce the high-iron containing spinel.

[0074] The Raman analysis showed that the spinel band intensity was the lowest for Alloy N06693 after 2900 h exposure in the environment used in the study at 593° C. and 14.3 atm, indicating that the incubation time for the onset of metal dusting for this alloy will be significantly greater than most of the others studied in this program.

[0075] In accordance with the principals of the present invention, a non-limiting model explains the function of aluminum to resist metal dusting corrosion as shown in (FIGS. **18**A and **18**B) as discussed hereinbefore. There may be defects in oxide scale that develop on surface of alloys. When carbon deposits on surface of alloys during exposure to metal dusting environment, carbon diffuses through these defects and reduce the spinel phase to Fe_3C and/or Ni metal. These particles form channels for transferring carbon through oxide scale. Oxygen may also diffuse through the channels resulting in formation of additional chromium oxide. However, the carbon diffusion rate is probably higher than that of oxygen and formation of additional chromium oxide beneath the carbon channel may not be feasible. Therefore, carbon can continue to diffuse into alloys through the channels and finally form dusting pits. When aluminum is added to the alloy, alumina scale usually forms underneath chromium oxide scale. There may be two effects of alumina to resist metal dusting corrosion. First, the carbon transferred through the channel may not be able to penetrate through alumina layer because alumina is much more stable than spinel. Second, the partial pressure of oxygen to form Al_2O_3 (3.6×10^{-57} atm) is much lower than that of Cr_2O_3 (2.6×10^{-37} atm) at 593° C. A thin layer of alumina scale can form (even with limited oxygen transport through the channel) beneath the carbon diffusion channel, thereby reducing the growth of metal dusting pits.

[0076] It should be understood that various changes and modifications referred to in the embodiment described herein would be apparent to those skilled in the art. Such changes and modifications can be made without departing from the spirit and scope of the present invention.

1. An article of metallic material manufacture for reducing susceptibility to metal dusting degradation, comprising a nickel base alloy comprising (in weight percentage) Cr of about 22-29, Al of about 2.0-3.5, Fe of about 0-1.0; Ti of about 0-0.3, Zr of about 0.1-0.2, Y of about 0-0.1 and the balance Ni.

2. The article as defined in claim 1 wherein the nickel alloy contains iron less than about one percent.

3. The article as defined in claim 1 further including a multi-layer tubing for passage of material therein and said tubing including a copper layer adjacent said nickel base alloy.

4. The article as defined in claim 3 wherein the multi-layer tubing includes an in-situ-developed chromium oxide layer.

5. The article as defined in claim 3 further including an aluminum oxide layer disposed adjacent the chromium oxide layer.

6. The article as defined in claim 3 wherein the multi-layer tubing further includes at least one of an aluminum oxide layer, a Fe $(Cr_{1-x}Fe_x)_2O_4$ layer with high chromium to iron ratio, and a substrate consisting essentially of copper, a Ni-based alloy layer and an Fe-based alloy layer.

7. An a multi-layer article of manufacture having a metallic layer with reduced susceptibility to metal dusting degradation, comprising:

a tubing having multiple layers, the multi-layer tubing having a hollow passageway allowing for passage of material therein; and

said multi-layer tubing including a copper alloy layer having a composition including at least copper; and

said nickel alloy layer comprising (in weight percentage) Cr of about 22-29, Al of about 2.0-3.5, Fe of about 0-1.0; Ti of about 0-0.3, Zr of about 0.1-0.2, Y of about 0-0.1 and the balance Ni;

wherein said copper layer is positioned in said multi-layer tubing such that it will be exposed to a metal dusting degradation environment

8. The article as defined in claim 7 wherein the copper alloy layer is the innermost layer of the multi-layer tubing.

9. The article as defined in claim 7 wherein the copper alloy layer is bonded to the nickel alloy layer.

10. (canceled)

11. The article as defined in claim 7 wherein the multiple layers are selected from the group consisting of bonded layers and unbonded layers.

12. The article as defined in claim 7 wherein the multi-layer tube has at least two bonded layers and at least one of the bonded layers is comprised of a low melting point metal.

13. The article as defined in claim 12 wherein the low melting point metal comprises at least one of zinc, silver, tin, and cadmium.

14. The article as defined in claim 7 wherein the thickness of the copper alloy layer is greater than about 0.1 mm.

15. The article as defined in claim 7 wherein the copper alloy comprises weight percentages of copper in the range of about 50-90, aluminum about 2-20, and nickel about 4-20.

16. The article as defined in claim 15 further comprising an oxide layer including at least one of in-situ-developed Cr2O3 and FeCr2O4.

17. The article as defined in claim 7 wherein the nickel alloy layer further includes aluminum.

18. An article of manufacture for reducing susceptibility to metal dusting degradation, comprising:

a multi-layer metallic component for use in a corrosive atmosphere the component containing carbon.

19. The article as defined in claim 18 wherein the multi-layer metallic component further includes at least one of a Ni alloy and an Fe alloy layer.

20. The article as defined in claim 18 wherein the multi-layer metallic component further includes a cobalt alloy layer and no nickel alloy layer or iron alloy layer.

* * * * *